

Date: June, 1st, 2016

Category: Bachelor Thesis

Email: cacos13@student.sdu.dk

Use of MEMS Biosensors for Detection of Biogenic Amines



Author:

Carlos André Bravo Costa

Supervisors:

Jacek Fiutowski

Roana Melina de Oliveira Hansen

Robert Brehm

In cooperation with the Mads Clausen Institute SDU Sønderborg, NanoSYD, Fraunhofer
ISIT, AmiNIC APS.

Mads Clausen Institute, University of Southern Denmark, Alsion 2

DK-6400 Sønderborg

Phone: +45 6550 1690

Fax: +45 6550 1635

Acknowledgments

I would like to thank Fabian Lofink from the Fraunhofer Institute for Silicone Technology (ISIT) for kindly providing the test and functionalized on-chip S-CF-EV cantilevers used as base for the development of this thesis and for the valuable data. To the MCI and NanoSyd Institutes for giving me access to the needed infrastructure and materials. A huge thanks to Kasper Paash, Wai Keung Mo and Lars Dugen, lecturers at the Mads Clausen Institute, for the invaluable orientation provided during the development phase.

My final thanks will go to my supervisors, Roana Melina de Oliveira Hansen, Robert Brehm, Jacek Fitowski, to my family, my friends and co-workers for all the support, inspiration and motivation given during the development of this thesis.

Thank you all!

Sønderborg, 1st of June 2016

Carlos Andre Bravo Costa

Abstract

Within the scope of the 6th semester Bachelor project, a qualitative assessment is made to determine and compare the sensitivity accuracy and price of different possible setups using micro-cantilever MEMS biosensor as an early identification method for the presence of specific biomarkers. This is achieved by measuring the small changes in resonance frequency of the cantilever, while focusing on the miniaturization process, on the mechanical action of the cantilever and on the electronics and optics necessary to support them. The objective will be to propose the design of a portable device that could be further adapted for applications in the food industry or biomedical fields, both as a quality control tool in food related industries and as an early diagnostic tool for healthcare-associated infections.

Table of contents

<u>1</u>	<u>THESIS FORMULATION</u>	<u>1</u>
1.1	PROJECT BACKGROUND	1
1.2	STATE-OF-THE-ART	2
1.3	PROBLEM STATEMENT	3
1.4	OBJECTIVE	3
1.5	REQUIREMENTS	4
1.6	METHODOLOGY	4
1.7	DESIRABLES	5
1.8	LIMITATIONS	5
1.9	DELIMITATIONS	5
1.10	EXPECTED OUTCOME	6
<u>2</u>	<u>INTRODUCTION</u>	<u>7</u>
2.1	MEMS AS BIO-SENSORS	7
2.2	ATOMIC FORCE MICROSCOPY	8
2.3	DRIVING MODES FOR CANTILEVER BEAMS	11
2.4	READING METHODS	12
2.5	SELF-SENSING PIEZOELECTRIC CIRCUIT AS A READ-OUT METHOD	13
2.6	OPTICS AS A READ-OUT METHOD	14
2.6.1	LASER MODULE	15
2.6.2	CANTILEVER MODULE	16
2.6.3	PHOTODIODE MODULE	19
<u>3</u>	<u>EXPERIMENTAL SETUPS</u>	<u>22</u>
3.1	PIEZOELECTRIC CANTILEVER BEAMS	22
3.2	OPTICAL SETUP	28
3.3	PIEZO SENSING	35
<u>4</u>	<u>FINAL TESTS AND RESULTS</u>	<u>40</u>
4.1	SETUP DESCRIPTION	40
4.2	RESULTS	42
4.2.1	PIEZO SENSING CIRCUIT	42
4.2.2	OPTICAL SETUP	45
<u>5</u>	<u>CONCLUSION</u>	<u>47</u>
5.1	SETUPS COMPARISON	47
5.2	RISK ASSESSMENT	50
5.3	FINAL CONSIDERATIONS	52
<u>6</u>	<u>REFERENCES</u>	<u>53</u>
<u>7</u>	<u>APPENDICES</u>	<u>55</u>
7.1	QUADRANT PHOTODIODE RECOMMENDED CIRCUIT	55
7.2	COMPARISON OF ISOLATION TRANSFORMERS	56
7.3	BEAM RESONANCE IN ANSYS	57
7.4	MATLAB CODE	77

7.5	RISK ASSESSMENT	87
7.6	GANTT CHART	89

1 Thesis formulation

1.1 Project background

The Bachelor project is the focus of the 6th semester for the students of the Engineering program of Bachelor of Science in Mechatronics at the Mads Clausen Institute (MCI) at the University of Southern Denmark. It is designed to challenge the students in demonstrating an overall view independence and mastering of the core skills taught during the study programme. This is a working process that shall document the student's engineering-specific competencies attained during the process within a limited, course-relevant and engineering specific subject. The selected problem can be investigated from a theoretical, experimental or practical point of view. [4].

Within this scope, an opportunity was identified for the development of a project within the applications of Microelectromechanical Systems (MEMS) for the detection of organic chemical molecules. This technology allows unparalleled synergy between previously unrelated fields such as biology and microelectronics, having today several applications in the field of medicine mainly as pressure or chemical sensors in blood pressure monitors, catheters, respirators, blood analysers, and hospital beds, among many others [11]. Considering my previous experience and education as a healthcare professional, it was within my wishes to explore and relate both of my fields of knowledge.

The MCI, from the University of Southern Denmark has been previously working on the proof-of-concept for using micro-cantilevers as biosensors for the detection of cadaverine, a diamine product of protein hydrolysis, using a non-invasive approach.

In the food industry safe food is an important matter since access to sufficient amounts of safe and nutritious food is a key to sustaining life and promoting good health. The ingestion of unsafe food can cause more than 200 diseases, that affect millions of people annually including many children. Food safety, nutrition and food security are inextricably linked, that can impede socioeconomic development by straining healthcare systems and harming national economy, tourism and trade [20].

Biogenic amines are promising candidates as meat safety biomarkers, and when ingested can have several physiological and toxicological effects for the human body. Parallel to this

research there is a close collaboration between the institute and the South Jutland Hospital in Sønderborg for bacteria measurement applications.

Bacteria like MRSA, C. Diff. and E. Coli are responsible for most of nosocomial infections and annually in the USA, these cause approximately 2 million patients to suffer with healthcare-associated infections (HAIs) and nearly 90,000 patients die as a result. The overall direct cost of HAIs to hospitals ranges from 28 to 45 billion dollars, being most HAIs actually preventable or their morbidity and economical outcome minimized if vectors and/or ongoing infections are early identified [3].

Could then the previous setup of a micro-cantilever MEMS biosensor be adapted to be used as an early identification method for the presence of such biomarkers while being smaller, quicker and cheaper than the current state-of-the-art setup, preventing the huge economical costs and more importantly, the costs in human lives?

1.2 State-of-the-art

There are several biochemical techniques used as diagnostic tools in medicine or as quality control check in various industries like the food industry, which besides being quite well known and used on the market, they are considered to be highly sensitive and with strong detection specificity. From the most common used techniques there is the enzyme-linked immunosorbent assay (ELISA) for bacterial or viral assays detection with some applications in the food industry for the detection of allergens, where antigen or antibody quantification can be done in the microgram or even nanogram levels. As alternative solutions there are also different specific chemical tests that are less accurate or sensitive and require predefined incubation periods [5].

For the detection of biogenic amines such as cadaverine, many standard chromatographic techniques have been described for identification and quantification, such as gas phase chromatography are used as quality-control check in the food industry and have been described for its identification. However, their use requires specialized staff to be operate, and such setups are usually quite expensive and bulky as is the example in gas phase chromatography. Qualitative methods such as using the sense of smell can be unreliable for small amounts of biogenic amines and dependent on external environmental factors [14].

1.3 Problem Statement

Micro-cantilevers could be an option to replace the state-of-the-art methods, since it can overcome some of its issues. At the University of Southern Denmark (SDU), the Mads Clausen Institute group has been working on the proof-of-concept for sensing cadaverine via various non-invasive methods. At the moment micro-cantilevers are functionalized with specific molecules applied to their surface, these act as binding agents when in contact with samples of the targeted organic molecules. The binding effect will alter the mass of the micro-cantilever and change its resonance frequency.

The objective of this bachelor project will be to determine and compare the sensitivity of different possible setups in measuring the small changes in resonance frequency of the cantilever, while focusing on the miniaturization process, on the mechanical action of the cantilever and on the electronics and optics necessary to support them.

This work will be used as proof-of-concept, with the objective of further refining it towards the detection of specific organic molecules. Also, simply by changing the binding agent on the functionalized cantilever and making it an antibody-sensitized microfabricated cantilever, a portable device could be further adapted for applications in the biomedical field as, for example, an early diagnostic tool for healthcare associated infections.

1.4 Objective

The ultimate aim of this thesis project will be to build a functional prototype(s) and test its viability for detection of a desired organic molecule by measuring changes on the resonance frequency of functionalized microcantilevers after exposure to the target biomaterial. The project has to be fulfilled by the 01.06.2016, where a functional test setup(s) and bachelor thesis report on the findings from the experimental measurements must be handed in.

The prototype requires the development of different electronic/optical setup builds, for measuring the resonance frequency changes of functionalized cantilevers (when exposed to target molecules) which are given an excitation signal using a piezoelectric transducer connected to a signal generator. This project will investigate and compare different methods for performing these measurements, for example optical and piezoelectric based techniques.

By the end of the project, an evaluation on each method's sensitivity and miniaturization feasibility will be performed, opening the door for future upscale fabrication of such biosensors.

1.5 Requirements

The following requirements are to be met:

- The finished device must be able to be smaller than previous setups;
- Analyse and compare different potential methods with respect to accuracy/sensitivity against present setups;
- The molecules applied on the cantilever that work as a binding agent must be able to sensibly detect cadaverine molecules and/or specific bacteria activity products;
- The finished device must have a cantilever design easily removable/replaceable from the piezoelectric transducer, by simple mechanical means.

1.6 Methodology

In order to develop such a device, a literature review is initially made on typical setups used in current research and state-of-the-art. A morphological analysis of each setup is performed, while comparing expected price, accuracy and sensitivity of each.

Posteriorly to the analysis of current setups limitations and discussion with supervisors for possible improvements, a component choice is made as a first step proposal for future miniaturized designs and assembled into the required experimental electro-optical setups.

Two examples of methods that could be tested are optical and piezoelectric based. In the first setup by using a visible laser diode emitting a beam that would hit the cantilever by the means of a lens system, and the resulting beam would be reflected into a quadrant photodiode, making it possible to determine the resulting frequency of the cantilever. On the second setup the same functionalized cantilever is given an excitation signal via a piezoelectric transducer and then, after being disturbed from its equilibrium position, by the means of a switch circuit the piezoelectric transducer is left to itself, oscillating with decreasing amplitude. Due to the difference in mass of the cantilever the resulting frequency could be then measured inferring the amount of the target organic molecule that has bound itself to the functionalized cantilever.

The individual setup(s) are then compared for their sensitivity, accuracy and price in correlation with minimization means.

1.7 Desirables

With support of the supervisor's team:

- Extra funding for this Bachelor project will be procured by application to a grant from the Siemensfonden for material and operational costs, and also from other local companies that could be interested in the development of such project;
- Possible collaboration with an external company, AmiNIC APS as support for the miniaturization process of the device.

1.8 Limitations

During the thesis project process and development of the prototype, I will be subjected to the following limitations:

- The course objectives restrict the budget to 2000 DKK from own SDU funding;
- The project process is constrained to 4-month period from the 1st of February 2016 to the 1st of June 2016;
- This thesis will be developed by a single student being limited in resources and thereby man hours.

1.9 Delimitations

- Due to the project time frame, even if proof-of-concept is achieved it is not aimed at the full development of the optical laser setup, so off-the-shelf components will be preferred;
- The binding agent used to be applied for the cantilever will not be the aim of this thesis development, therefore already proven recipes will be used as the best approach;

- Due to the project time frame, I will not conduct a full market research, against other state of the art methods of detecting organic molecules, being the focus on proof-of concept;
- Material and facilities provided by SDU will be preferred for research, development and testing the experimental setup, due to its close proximity and well known infrastructure and logistic processes.

1.10 Expected Outcome

- The finished device must be able be smaller than previous setups, aiming for future portability;
- The molecules applied to functionalize the cantilever as binding agents, must be able to sensible detect cadaverine molecules or specific bacteria activity products;
- The finished device must have a cantilever design easily removable/replaceable from the piezoelectric transducer, by simple mechanical means;
- A comparison between setups must be made regarding limitations, sensitivity and costs;
- Proposal of future improvements for a possible miniaturized design.

2 Introduction

This section is an overall look into the use of MEMS as sensors compared to the previous work done at the MCI. This is reflected as the initial decision matrix based on bibliography research that results in the choice concepts to be further developed as prototypes. A risk assessment and a Gantt chart for the overall development of the bachelor project can be found in appendix 7.5 and 7.6 respectively.

2.1 MEMS as bio-sensors

The use and development of cantilever beams as sensors took place in the last 16 years, favouring a new line of cheap, small, fast sensors with “on the field” pertinence for environmental monitoring or point of care diagnostics. The specific properties of those sensors make possible to measure quantities or phenomena that otherwise would be difficult or expensive to achieve. Such microelectromechanical systems rely on optical and electrical means for signal transduction and its applications, as previously mentioned in the earlier chapter, range from drug research, to use as diagnostic tools in medicine, as quality control check in the food industry, or even for explosives detection [21].

It is taken as a starting point for the development of this thesis the previous work done at the MCI for functionalizing micro-cantilevers in meat degradation measurements.

Stoney studied the tension of metallic films, and described it in an equation as means of calculating film stress σ_{film} , from the change of curvature by using the young's modulus E_s , the poisson ratio ν_s , the thickness of the film h_f and substrate h_s and \mathcal{K} the curvature of the system [7]:

$$\sigma_{film} = \frac{E_s h_s^2 \mathcal{K}}{6 h_f (1 - \nu_s)} \quad (1)$$

Such type of cantilever beam systems can be generically described by a purely mechanical point of view as spring-mass-damper systems, where the spring constant k is related to the dimensions, width w , height h , length l and material properties (Young's Modulus E) together

with moment of inertia of the cantilever [6]. Further simplification, makes this relation expressed as it follows:

$$k = \frac{Ewh^3}{4l^3} \quad (2)$$

Furthermore, a relation between the force applied at a passive cantilever beam and the resulting surface stress can be found.

$$F_{applied} = \frac{\sigma_{surface}wh(1 - \nu)}{l} \quad (3)$$

With ν being the Poisson ratio of the material of the beam.

This means that film stress changes can be measured experimentally from curvature changes, by taking the approximation that they are uniformly distributed in the desired system.

Cantilever beams can be designed in different size and shapes depending on the intended applications and the subject of many research papers. For simplicity it was chosen the basic rectangular cantilever, as previously supplied by SDU partners like Fraunhofer ISIT.

2.2 Atomic Force Microscopy

The principle described in the previous section was the approach taken by the MCI with the use of Atomic Force Microscopy (AFM) together with silicon-gold-coated cantilevers. The cantilevers were functionalized with a cadaverine binding element (cyclam) and later exposed to this bio-amine while being driven at resonance frequency. With AFM it was possible to measure the resulting changes in bending and shifts in frequency related to the mass change of the cantilever when bound with cadaverine molecules

This relation between mass and frequency change is described by the following equation:

$$\Delta m = \frac{k}{0.96\pi^2} \left(\frac{1}{f_0^2} - \frac{1}{f_1^2} \right) \quad (4)$$

As it can be seen the mass variation is related to the spring constant of the cantilever k , f_0 the initial value at resonant frequency and f_1 the resulting frequency with mass change. [1].

In this study it was found that for a simple rectangular micro-cantilever of $130\ \mu m$ length a change of mass in the order of $674 \pm 198.3\ fg$ would originate a shift in the resonance frequency of about $0.85 \pm 0.25\ kHz$ [8].

To minimize this working setup and making it more cost effective it is needed to look into more detail on how the AFM fundamentally works and with this understanding decompose it to its basic working elements.

AFM uses a sharp triangular tip connected to a cantilever beam that deflects according to the topography of a surface, like it can be seen in the following picture.

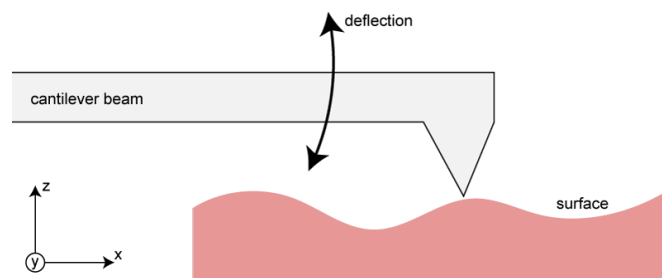


Figure 1 - AFM working principle

The deflection of the cantilever beam is then measured by Optical Beam Deflection(OBD). This method uses a laser source that projects a beam at the cantilever tip, and reflects back back into a photo diode module that will measure displacement according to the beam's movement.

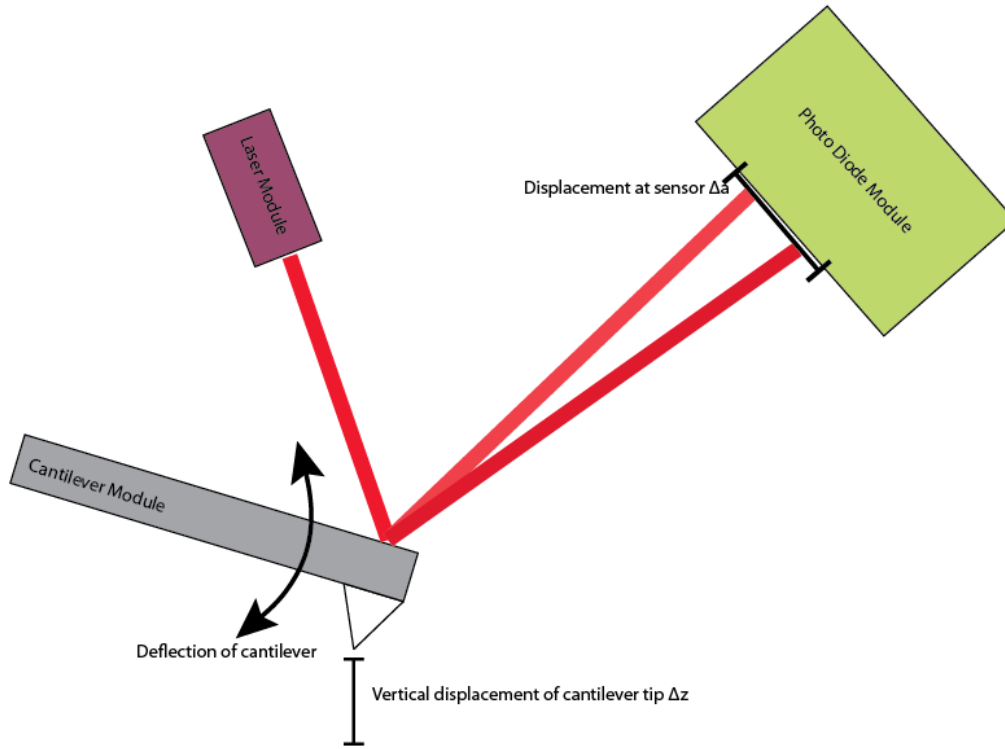


Figure 2 – Optical Beam Deflection

It is noticeable in the previous picture that the 3 distinct modules, the cantilever module, laser module and photodiode module, are the key components for an AFM like setup. The displacement of the laser beam at the sensor $\Delta \alpha$, can be described in relation with the vertical movement of the tip of the cantilever Δz , as it follows:

$$\Delta \alpha = 3 \frac{s}{l} \Delta z \quad (5)$$

Where s is the distance between the cantilever tip and the photodiode and l the length of the beam [18].

2.3 Driving modes for cantilever beams

The rectangular cantilever beam can be used passively where a change in mass would be given directly by a change in the applied force at a section of the cantilever or actively by driving it at resonance frequency and calculate mass variations from the shift in resonance.

The following table compares both methods.

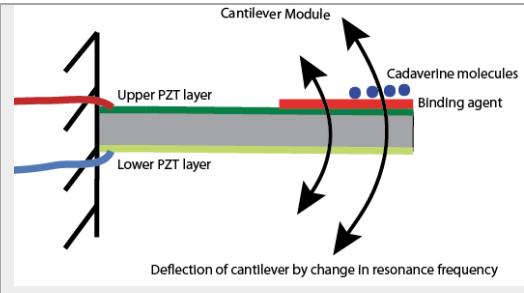
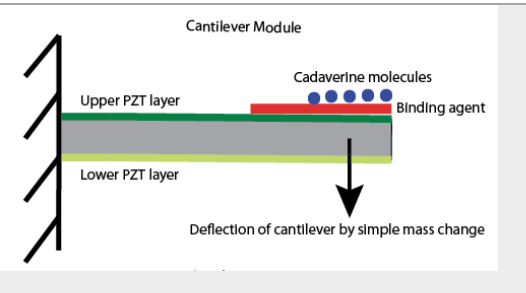
Modes	
<div style="display: flex; justify-content: space-around;"> <div style="text-align: center;">  <p>Figure 3: Cantilever module activated at resonance frequency (dynamic)</p> </div> <div style="text-align: center;">  <p>Figure 4: Cantilever module with passive activation (static)</p> </div> </div>	
Pros	Only bound molecules can cause mass change that will shift the resonance frequency
	Less initial components
	Easier to read deflection by optical and electronic means
Cons	Higher accuracy expected
	More components initially required
	Sensitive to environmental effects like air pressure and flow, temperature, among others
	Harder to read by optical means
	Less accuracy expected

Table 1: Comparison between active and passive methods

It can be seen that having the cantilever module being run at resonance frequency would be beneficial since at first glance gives a higher expected accuracy. Only molecules bound to the functionalized layer of the cantilever will cause a shift in frequency, not being influenced by a simple laminar flow of air [2]. Also according to Evtugyn 2014 [6] “*The static measurement mode can be used for aqueous sensors, whereas dynamic sensors are preferably used in the air or in vacuum*”.

Even if this method requires a signal to be supplied to the cantilever module and possibly a more complex circuitry, the fact that it is recommended for applications in the gas phase like for the detection of cadaverine, its gains in sensitivity and application for optical setups makes it a better choice.

2.4 Reading methods

Different reading methods can determine changes in frequency or mass of a rectangular cantilever. Five different read methods were selected as being the ones easier to achieve within the referred limitations and delimitations of this bachelor thesis. Each can present different challenges, that are further explored in the following table.

Reading methods					
	Simple optical	Integrated optics	Piezoelectric	Piezoresistive	Piezocapacitive
Pros	Simple approach based on the AFM setup,	Can be applied to arrays of cantilevers	Well known and studied	Applications for arrays of cantilevers	Applications for small sized cantilevers (nanometer scale)
	Works with cantilevers with good optical quality	Sensitivity compared to simple optical setup	Can be used both for actuation and reading	Can be used with a high range of media	Reading does not affect mechanical properties
	Can measure mass, surface and bulk stress	Can measure mass, surface and bulk stress	Can measure mass, surface and bulk stress	Can measure mass, surface and bulk stress	Can read mass
	Medium cost		Low fabrication cost	Medium cost	
Cons	Can't be used in small sized cantilevers (nanometer scale)	High fabrication cost	Cleanroom compatibility can be an issue	Piezoresistive layer can affect mechanical properties of the cantilever	High fabrication cost
	Sensitive to changes in refractive index	Sensitive to changes in refractive index	Easier application for dynamic measurements		Very sensitive to parasitic capacitances
	Hard to be applied to arrays	Complex microfabrication			Requires extra components for circuitry
					Complex microfabrication

Table 2: Comparison between reading methods adapted from Boisen et al.

By analysing the table above, the methods with high fabrication cost were discarded since it could not be found that they give a significant advantage over the lower cost methods.

Furthermore, the final choice relied on the simplest methods available, with lower costs and similar sensitivity. The simple optical method and the piezoelectric method are based on well-known applications using simpler setups, while at the same time providing much different approaches to solve the same problem (optical vs piezo sensing) when compared to the remaining piezo solutions.

2.5 Self-sensing piezoelectric circuit as a read-out method

As mentioned in Table 2, the piezoelectric solution for a read out would allow for a piezoelectric actuator to drive the cantilever beam at resonant frequency. At the same time a second layer could be use as sensor. This is due to the specific properties of piezocrystals that when subjected to mechanical pressure produce an electric potential (sensor effect). On the other hand, when an electric field is applied the crystals in the piezo reorient themselves, which results in mechanical deformation (actuator effect).

A circuit was needed that would amplify the resulting signal. Since only the shift in resonance frequency is of interest, it should be able to compare the cantilever value against a reference. Two setups were found as being the most common for this type of application from literature review [12].

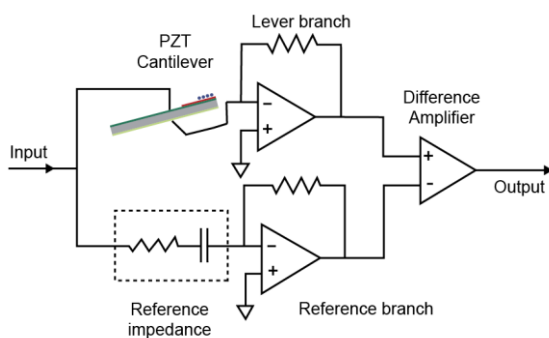


Figure 5: Voltage bridge setup based on Miyahara et al, McGill University

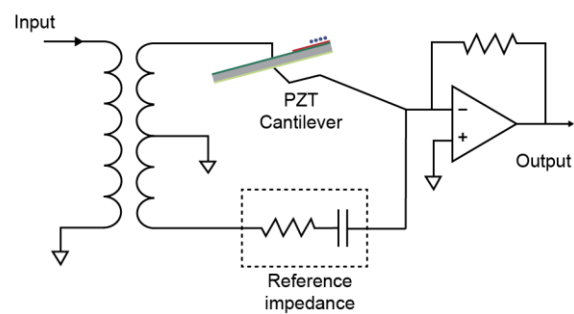


Figure 6: Current bridge setup based on Miyahara et al, McGill University

Both circuits act in a similar way. An input is fed to the circuit, that signal will change after with the shifts of resonance frequency after it goes through the cantilever with. That signal is then again compared against a reference, and that difference would be the desired resulting output.

By taking a closer look at *Figure 5*, this voltage bridge setup circuit takes two amplifiers that increase the signal output from the piezo cantilever and the reference branch and then compare both outputs by the use of a difference amplifier. For the current bridge setup in *Figure 6* an isolation transformer is used to separate the piezo-sensing system from artefacts originated from the driving signal, suppressing electrical noise. The current that goes through the operational amplifier will be resulting from the difference with the constant value that travels to the reference impedance branch and the change in current caused by the shift in resonance frequency of the cantilever. An operational amplifier is then used as a current to voltage converter, by knowing the value of the resistor used in the negative feedback it is then possible to determine the current by simple use of Ohms' law. This would make way for the output to be read, for example, by simple ADC from a microcontroller, which is important when we think about the miniaturization process of a future device. It is also noticeable that this circuit design uses less components, making it simpler and cheaper to build. This means also that there is less dependence on the components that could affect the sensitivity of the circuit, like is the case of the frequency and phase response of the operational amplifiers used in the voltage bridge circuit [12].

It becomes then a simple choice to use the circuit shown in *Figure 6* as one of the setups for a prototype of a self-sensing circuit using the piezoelectric effect.

2.6 Optics as a read-out method

As earlier mentioned, a simple optical setup based on AFM is one of the chosen read out methods to find shifts in resonance frequency of the cantilever beam.

As described 3 distinct modules are used in AFM, the cantilever module, laser module and a photodiode module. For an optical setup is then important to look with more detail into their functionality.

2.6.1 Laser module

In AFM the laser module has to follow certain requirements as it follows;

<i>Properties</i>	<i>Requirements</i>
<i>Optical power</i>	0 – 2 mW
<i>Wavelength</i>	650 ± 50 nm
<i>Intensity distribution</i>	Symmetric
<i>Pointing stability</i>	$\leq 4.6 \mu\text{rad}/K$
<i>Heat dissipation</i>	Minimal to minimize thermal deviations
<i>Size</i>	Minimal

Table 3: Requirements for AFM based on I. de Rijk recommendations

One of the lasers readily available at the SDU is the GLG5370 series from NEC. The main specs from its datasheet [17] can be found in Table 4.

<i>Type</i>	<i>GLG5370 series</i>
<i>Appearance</i>	
<i>Wavelength</i>	632.8 nm
<i>Output power</i>	> 1mW
<i>Polarization</i>	Linear
<i>Transverse Mode</i>	TEM ₀₀
<i>Beam diameter at 1/e²</i>	Approx. 0.65 mm
<i>Beam divergence</i>	Approx. 1.23 mrad
<i>Output power stability</i>	+/- 5% / 24H
<i>Dimensions and weight</i>	Diameter 40 x 265 length , 0.45 kg
<i>Power supply dimensions</i>	90x60x190 mm , 0.7 kg
<i>Power consumption</i>	Approx. 30VA
<i>CRDH classification</i>	III a

Table 4: Specifications from NEC HeNe gas laser datasheet for the GLG5370 series

By comparing optical power and wavelength, this HeNe laser provides the needed optical characteristics when compared to the requirements of AFM. There are other options such as

laser diodes, these are smaller, more efficient and cheaper. However, its optical properties are not as good when compared to the HeNe laser, it needs complex external optics, does not offer as good coherence lengths and it suffers from faster degradation over time [10].

Since as mentioned in this thesis delimitations, of-the-shelf components and materials already available at the SDU are preferred for testing a possible experimental setup. Therefore, since the GLG5370 from NEC meets the optical power and wavelength requirements of an AFM it was taken as a choice for a proof of concept and comparison prototype. However, for a future prototype, that would focus on the optical technology option only, the use of laser diode modules would be preferred, since it is ideal for a portability/miniaturization process.

2.6.2 Cantilever module

The cantilever module will reflect the laser source back into a detector. The following set of statements and equations describes the optics involved as according to *Pedrotti et al* [15].

The gold coated surface of the cantilever acts then as of a mirror. This effect can be seen in the following picture [19].

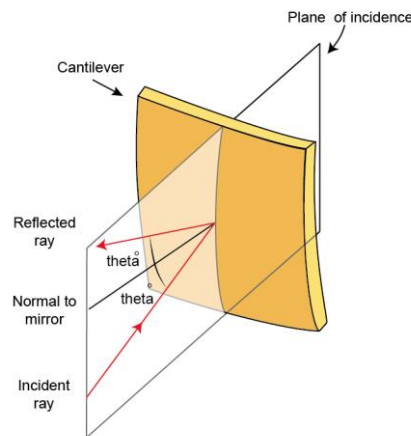


Figure 7: Reflection law effect based on Saleh and Teich, *Fundamentals of Photonics*

Typically a HeNe laser presents a Gaussian intensity distribution, $I(r)$ that can be described by the following equation:

$$I(r) = I_0 \exp\left(-\frac{2r^2}{\omega_0^2}\right) \quad (6)$$

Where ω_0 is the beam waist radius at which the intensity is down to $\frac{1}{e^2}$ of its value on the beam axis, I_0 . A Gaussian beam minimal waist is the minimal value of ω_0 , and the beam diameter reaches a minimum value d_0 .

$$d_0 = 2\omega_0 \quad (7)$$

The beam waist will still change with distance z . This variation of the beam waist with distance, $\omega(z)$ is described as:

$$\omega(z) = \omega_0 \sqrt{1 + \left(\frac{z}{z_0}\right)^2} \quad (8)$$

Where z_0 is the Rayleigh length as in the following equation, with λ being the wavelength of the radiation.

$$z_0 = \frac{\pi\omega_0^2}{\lambda} \quad (9)$$

As described earlier in Table 4 the chosen laser has a transverse mode TEM_{00} with a single even intensity profile, which means that ω_0 depends on the beam divergence angle θ .

$$\omega_0 = \frac{\lambda}{\pi\theta} \quad (10)$$

The radius of curvature (curvature at wave front) by distance $R(z)$ is given by:

$$R(z) = z \sqrt{1 + \left(\frac{z_0}{z}\right)^2} \quad (11)$$

For a clearer understanding, a visual representation of equations 6 to 11 can be seen in the following picture.

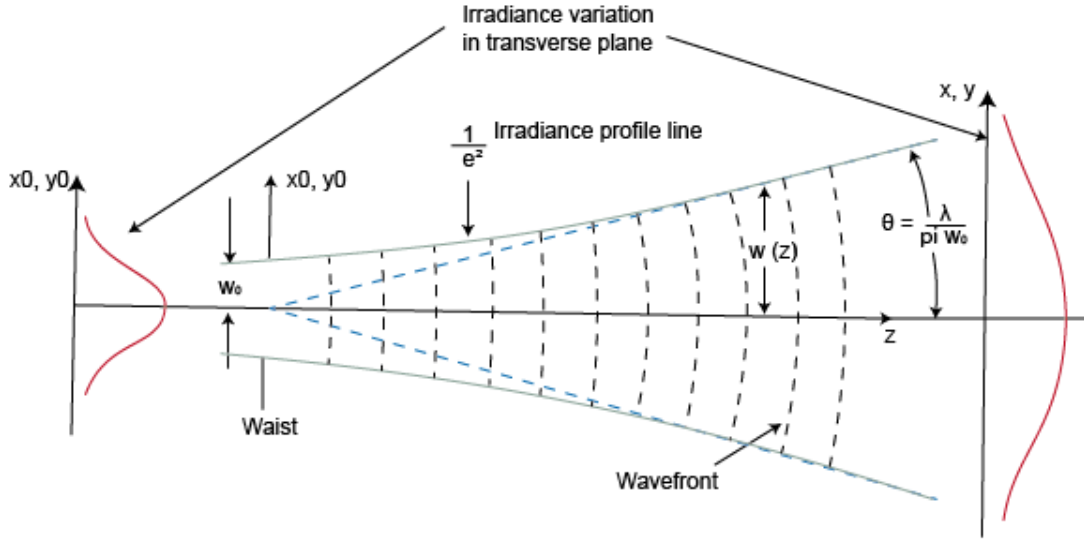


Figure 8 : Gaussian beam propagation based in Pedrotti et al, Introduction to Optics

A system of lenses will also be needed to make the beam spot to converge on the cantilever so it is mostly reflected by it and back into the photodiode. It is then necessary to take into consideration the effect of lenses in the setup and how they will affect the beam. The description of such geometry optics are done by the *Lens-maker's Equation* [15] and can be applied for thin lenses as it follows.

$$\frac{1}{f} = (n - 1) \left(\frac{1}{R_1} - \frac{1}{R_2} \right) \quad (12)$$

With f being the focal length of the chosen lens, n the refractive index of the medium that the beam goes through, R_1 and R_2 the radius of curvature of the lens. For converging lenses like shown in Figure 9 (positive) R_1 is of positive sign and R_2 is negative, making F positive and for diverging lenses like Figure 10 (negative) R_1 is of negative sign and R_2 of positive sign, making F negative.

This relation is more easily seen in the following figures [23].

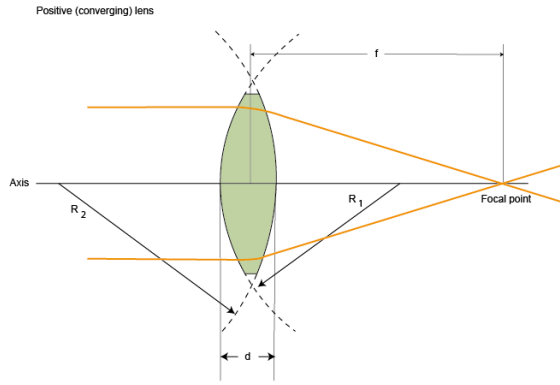


Figure 9: Schematic for converging lenses

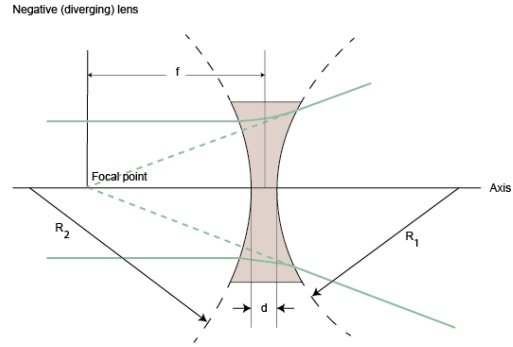


Figure 10: Schematic for diverging lenses

A pair consisting of a diverging and a converging lens can be used to focus the laser beam on the cantilever tip, by experimentally changing the distance between both lenses until the desired spot size is achieved ($200\ \mu m$ diameter, according to cantilever beam dimensions). This simulation is performed using a MatLab script that can be found in appendix in section 7.4.

2.6.3 Photodiode module

This final module is responsible for the detection of the displacement of the reflected laser spot at a distance, described earlier in equation 5.

In AFM this application is fulfilled by the use of quadrant photodiodes as it can be seen in Figure 11.

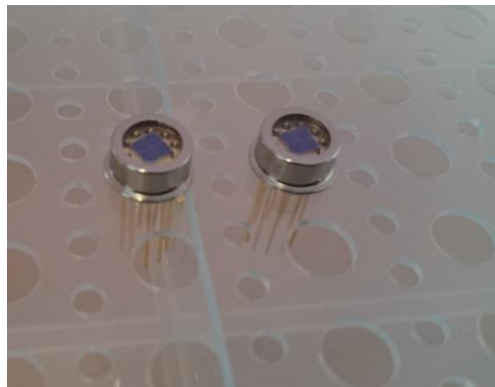


Figure 11 : Quadrant photodiodes units S4349 from Hamamatsu, available at SDU

The photodiodes as it can be seen in Figure 11 present 4 different photosensitive surfaces, with the beam pointed at its centre. For AFM setups the laser spot should overlap a portion of all segments of the photodiode at the same time, and should not exceed the outer boundaries of the quadrant photodiode. The laser source should have a beam of Gaussian intensity

distribution (which is accordingly in the case of our laser source), and should be sensitive for the required wavelength [18]. According to the datasheet, the photosensitivity peaks with wavelengths between 600 to 800 nm, which is correct for the selected laser source.

However, an amplifying circuit is required for the outputs of the 4 quadrants together with a mounting unit for the photodiode. The recommended circuit can be found in appendix A, but building such a circuit for a possible optical setup was out of scope for the development of this thesis as mentioned in its delimitations, therefore a complete of-the-shelf unit was needed. Such complete unit setups are however expensive, and can cost up from 3200 DKK per unit (ThorLabs). Taking into consideration the budget limitations of this thesis, external sponsorship from the NanoSyd institute and Siemensfonden was procured, without success. The development of the optical setup used a photodiode unit, already available at SDU, the UPD-500-UP.



Figure 12 : UPD-500-UP from Alphalas

This photodetector model presents the following specifications as seen in Table 5

Model	Rise time (ps)	Bandwidth (GHz)	Spectral range (nm)	Quantum efficiency @ peak	Sensitive area (Dia. $\mu\text{m}/\text{mm}^2$)	Noise equi. Power (W/√Hz)	Dark current (nA)	Material	Optical Input / Window type	RF output connector
UDP-500-UP	< 500	> 0.6	170 - 1100	90%	800/0.5	3.5×10^{-15}	0.01	Si	Polished, MgF ₂	BNC

Table 5: UDP-500-UP specifications

As it can be seen from the spectral range is adequate for the wavelength of the chosen laser source. The sensitive area diameter will pose a challenge since the reflected laser of the cantilever will have to hit its edge, and the displacement of the cantilever unit would cause the laser beam to shift into it. By using an oscilloscope, it then becomes possible to read the frequency at which the laser beam shifts into the sensitive area.

Also photodiode unit with similar specifications was previously used by *Ying Wang* [21] for the detection of cadaverine for an optical setup, applying the principle of the Michelson interferometer, but with problems regarding the unstable mounting of the cantilever to locate the reflection of the beam into an appropriate point. The use of a CCD camera to locate the beam's position and a stable setup for the cantilever mount that would allow freedom of movement in 3 axis could be an answer for the previously found issues, making the UPD-500-UP the initial choice for the photodiode module in an experimental setup.

3 Experimental setups

This section is an overall look into the development process of the chosen setups referred previously in the Introduction chapter. Firstly, it will cover the choice, calculations and necessary simulations for the cantilever beam unit since it will be commonly used in both setups. Secondly It will cover the simple optical read out method and the piezo-sensing method. All the calculations covered in this section are found in the MatLab code in appendix, in section 7.4.

3.1 Piezoelectric cantilever beams

As previously mentioned a simple rectangular cantilever being actively driven is chosen to be used as a sensor for the detection of bioamines. A portion of the cantilever is functionalized with a molecule binding agent based on a cyclam (2-ethxyethanol) solution which is specific to the target bioamine, cadaverine.

The Fraunhofer Institute for Silicon technology was contacted, due to previous partnership with the MCI. For the wanted application the use of S-CF-EV type cantilever beam chips was suggested (see Figure 13 and Figure 14).

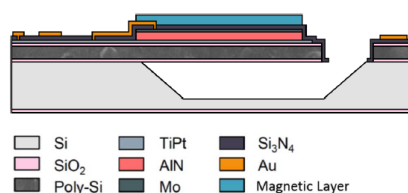


Figure 13: Single cantilever beam general composition. The piezoelectric layer is not specified but according to Fraunhofer it is always present on an Top and bottom layer and excluding the Poly-Si layer composition may vary from model to model

(image from Fraunhofer ISIT)

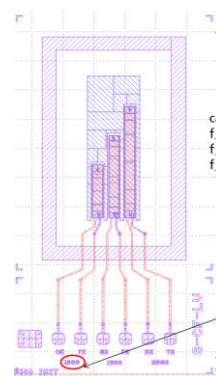


Figure 14: Cantilever chip aspect with three different cantilever lengths (image from Fraunhofer ISIT)

The cantilever chips possess 2 parallel cantilever beams. The supplied samples have 1500 μm length, 200 μm width, 12.5 μm thickness for the Poly-Si layer which compromises the

majority of its composition. These chips were mounted on a PCB with several connectors, each of them driving a corresponding piezoelectric layer.

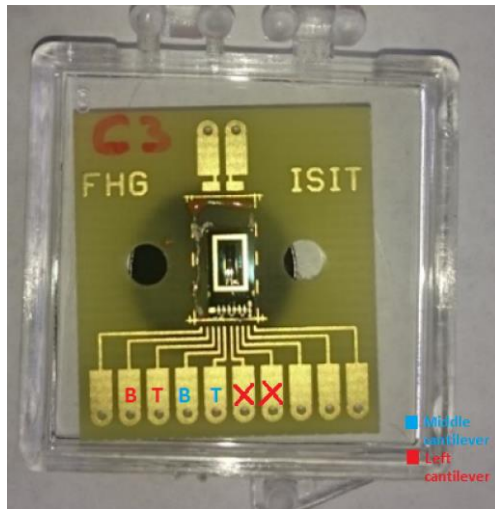


Figure 15 Cantilever chip on PCB with connectors schematic: B for bottom piezoelectric layer, T for top piezoelectric layer.

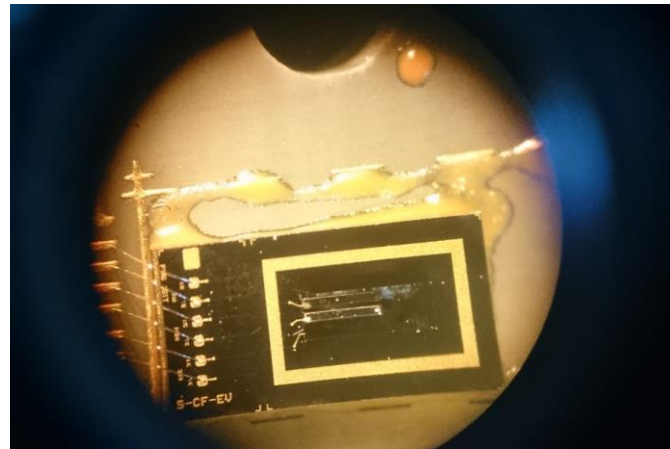


Figure 16: Cantilever chip on microscope where gold wire connections can be visible.

The remaining characteristics of each cantilever can be found resumed in the table below, as given by Fraunhofer ISIT.

S-CF-EV type cantilever 1500 μm lenght

Characteristic	Values
Youngs Modulus (Poly-Si layer)	170 GPa
Resonating frequency	7.8 kHz
Piezo electric voltage range	Usual: 10 V Safe: 0 - 50 V Possible: 50 - 100 V
Impedance at 8.5 kHz	80 $k\Omega$
Capacitance at 1 kHz	24.6 pF
Temperature range	"Operating temperatures up to several hundred degrees should be feasible"
Functionalized area	100 μm from tip

Table 6 : Main properties of the S-CF-EV cantilevers

With these initial values a model was built in ANSYS and simulated to find deflection and confirm resonance frequency values [9], the report of the different simulations can be found in appendix, section 7.3. The values are confirmed against calculations using the formulas described in section 2. Since these require several changes or adaptations to experimental values obtained during the development of the prototypes, a MatLab script was built to easily obtain them. The code for this script can be found in appendix, section 7.4.

The simulation and calculated results can be found resumed in the following tables, considering a mass change of 674 femtograms since this was the obtained previously in an AFM setup, and is used here as an approximation for calculation purposes.

Calculated parameters

<i>Parameter</i>	<i>Calculated values in MatLab</i>
<i>Spring constant</i>	4.5370e-05 N/m
<i>Cantilever mass</i>	1.8400e-12 Kg
<i>Final frequency of the cantilever after mass change</i>	7766.8e+03 Hz
<i>Surface area of cantilever (functionalized surface)</i>	3.0000e-07 m ²
<i>Force per unit area (of functionalized surface)</i>	2.1589e-07 N/m ² - Pa
<i>Deflection due to static mass change</i>	1.2973e-10 m
<i>Density of cantilever</i>	23.3966 kg/m ³
<i>Displacement of cantilever tip at resonance frequency</i>	4.0843e-09 m
<i>Displacement of cantilever tip at resulting frequency after mass change</i>	4.0532e-09 m

Table 7: Table of calculated values using MatLab R2016a

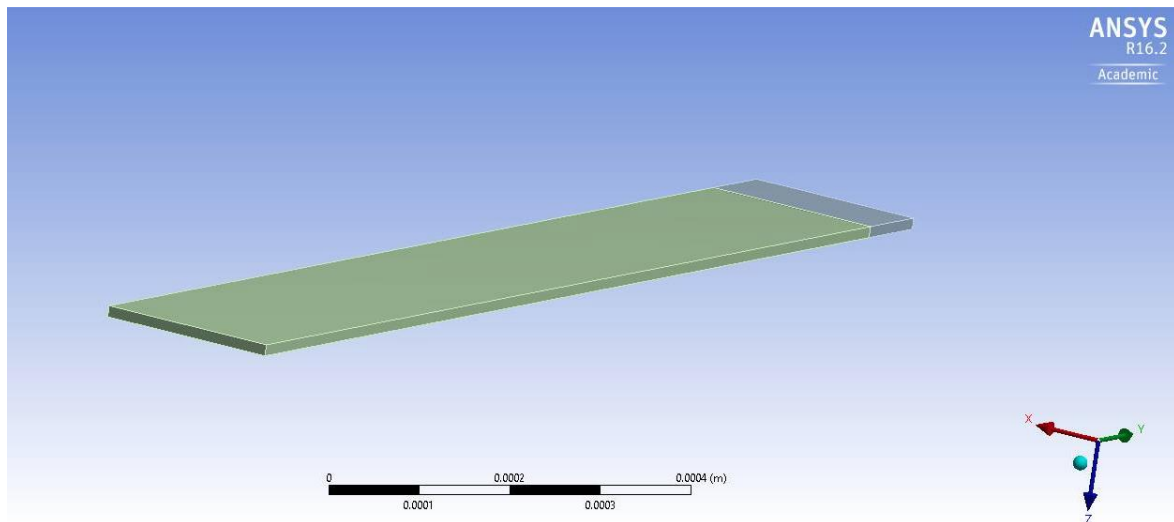


Figure 17: CAD model of cantilever beam with functionalized area in grey

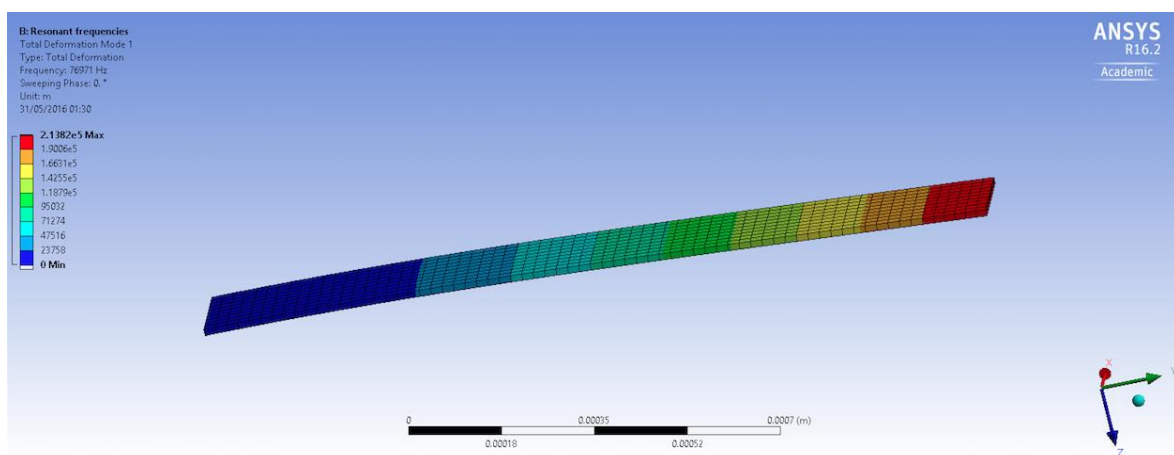


Figure 18: ANSYS MODAL analysis of cantilever beam

ANSYS simulation results (Modal – 2 Modes from 0 to 100 MHz)

Parameter	Value
Expected natural frequencies	76971 Hz
	482330 Hz
Expected natural frequencies with mass change (674 femtograms)Resonat	76968 Hz
	482100 Hz

Table 8: Table of simulated natural frequencies values using ANSYS R16.2

It is noticeable that the natural frequencies given by simulation are different from the given 7.8 kHz from Fraunhofer ISIT. In addition, the expected shift value in the frequency is quite small, of about 3 Hz for mode 1, which is against the calculated expected shift of 33.2 Hz (see MatLab code, section 7.4)

There are several possibilities that could justify the discrepancy in results. Both cases use the same material and beam specifications regarding Young's Modulus, Density and Poisson's Ratio. The last material property was taken from usual silicon-substrate materials, isotropic and linearly thermoelastic as being $\nu = 0.22$ [18], which could not be accurate. For simplification purposes the cantilever was approximated as being only composed of Poli-Si substrate, however its build can vary with the addition of other composite materials, that even if in small volume/quantities it could influence the obtained results. Another explanation could be that the boundary conditions are different from stated as seen in Figure 13 serves as a generic reference.

A simple test was carried out to see the response of exciting the upper piezo layer of the cantilever and measuring the corresponding output with an oscilloscope. At this point, an Hewlett Packard 54645D Mixed Signal Oscilloscope was used for the experiment, together with an AFG-2125 Arbitrary Function Generator from GW Instek.

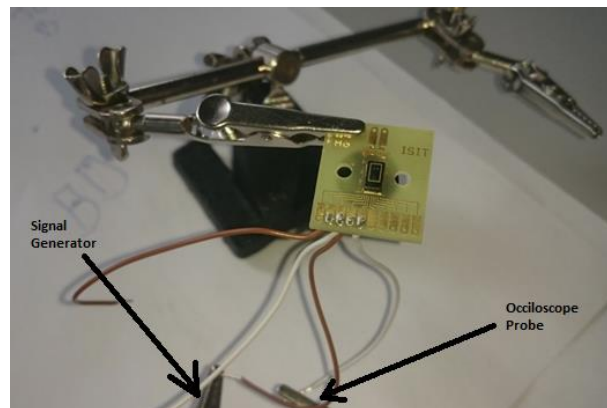


Figure 19: Piezo-cantilever connected to signal generator (upper layer) and to oscilloscope probe (lower layer)



Figure 20: Function generator, emitting a sine wave of 7.8 kHz, 10 V_{pp}

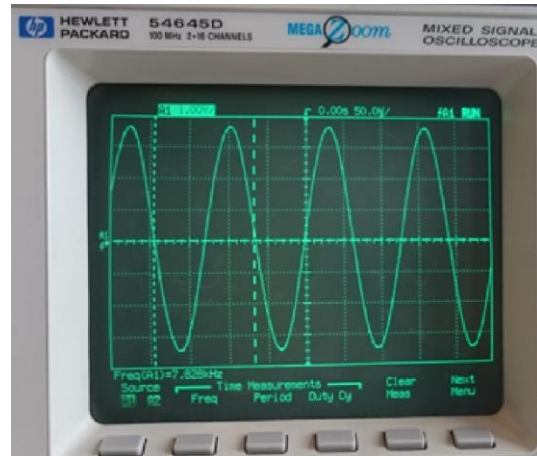


Figure 21: Oscilloscope reading a resulting sine wave of 7.828 kHz, 7.5 V_{pp}

As it can be seen there is a slight difference in the input and output for about 0.4% in frequency and 25% drop in V_{pp} . The signal generator was tested by directly connecting into the oscilloscope with no change in signal noted. Therefore, this difference can be probably explained by mechanical losses, and should be taken into account in the final result.

3.2 Optical setup

The optical setup experiment was carried on an optical table, with the laser beam travelling on the horizontal plane only, at 14 cm parallel to the table surface. The chosen HeNe laser source has an output power above 1mW as referred in section 2.6.1. For laser handling safety purposes this was brought down to the 0.742mW range by using a filter lens to reduce the beam power. The value was confirmed using a Power Meter as seen in the following images.



Figure 22: Laser source with Power Meter sensor after application of lenses



Figure 23: Output power result read in Power Meter

A pair of reflecting mirrors two dimensionally adjustable via precision knobs were used to redirect the laser to the free end of the table. The position of the laser beam was continuously confirmed by using a scaled ruler for optical tables so it would be kept at a 14 cm horizontal plane. The laser spot was measured to be approximately of 2 mm diameter.

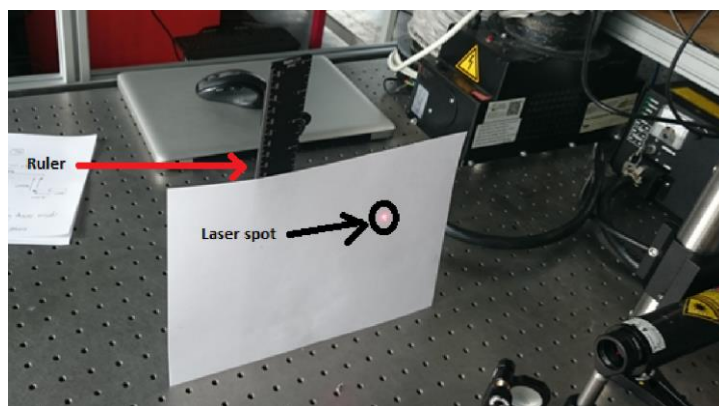


Figure 24: Laser calibration method with ruler and laser spot visible.

A simple test was used to verify the accuracy of the UPD-500-UP photodiode unit. A laser beam cutter running at a frequency of 1kHz was placed between the laser source and the photodiode as seen in figure Figure 25.



Figure 25: Beam cutter unit running at 1kHz (centre front). Photodiode unit with laser spot on sensitive area (right side)

The frequency output of the photodiode on a Hewlett Packard 54645D Mixed Signal Oscilloscope can be seen below.



Figure 26: Frequency response read at photodiode unit (1.003kHz)

This means a 0.3% difference in the measured result, which was considered acceptable for the required application.

As mentioned in section 2.6.2 of it was necessary to bring the beam spot down to the size of a single cantilever. This beam is reflected back to the photodiode that measures the shift in frequency. Several lenses types, kindly supplied by the MCI are seen in Table 9.

<i>Model</i>	<i>ThorLabs LC1715-A</i>	<i>ThorLabs LC1906-A</i>	<i>ThorLabs LA1708-A</i>	<i>ThorLabs LA1433-A</i>
<i>Shape</i>	Concave	Concave	Convex	Convex
<i>Coating Range (nm)</i>	350-700	350-700	350-700	350-700
<i>Diameter (mm)</i>	25.4	25.4	25.4	25.4
<i>Focal length</i>	-50	-27	200	150
<i>Index of Refraction n, at 633 nm</i>	1.515	1.515	1.515	1.515

Table 9: Lenses comparison table

The different pairs of concave and convex lenses were experimented on the setup. The LC1715-A paired together with the LA1433-A produce the desired effect as it can be seen in the output graphic of a MatLab simulation.

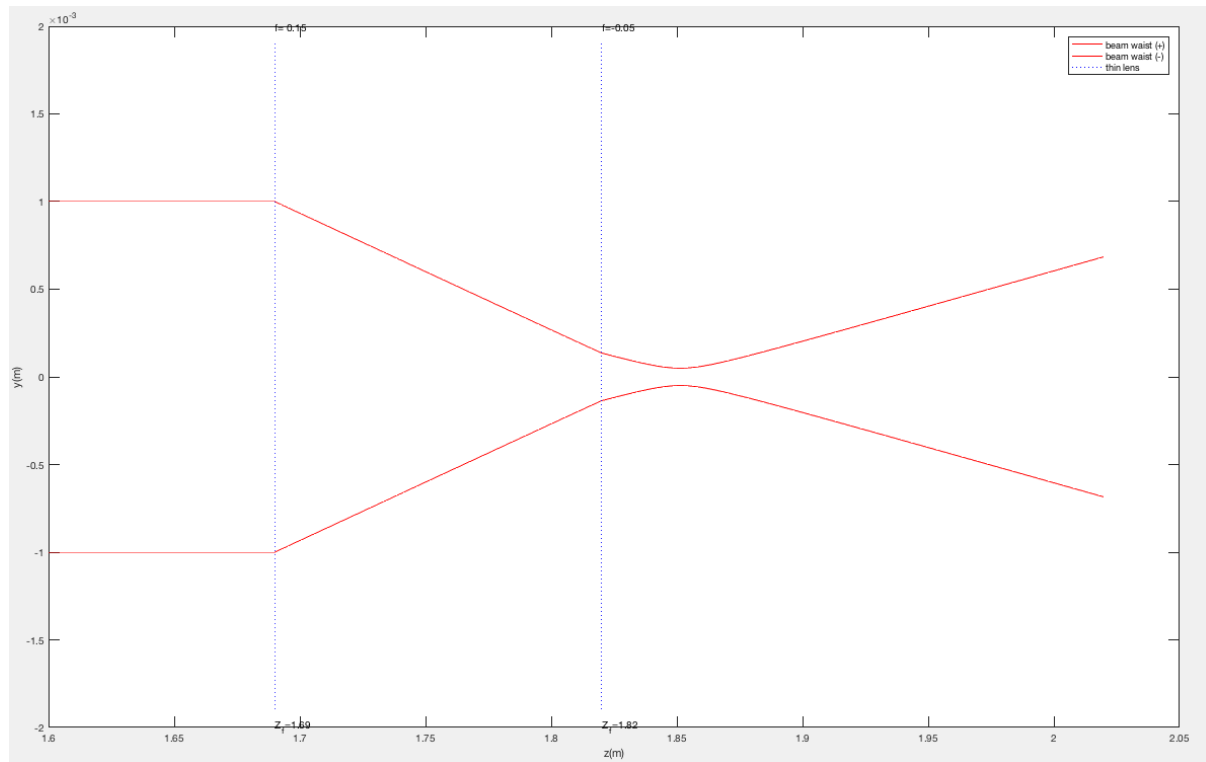


Figure 27: Graphic output of laser beam waist change over distance

As it can be seen, the waist of the beam reaches a minimal waist at about 31 mm from the last lens position. By increasing the distance at 10 mm steps and checking experimentally the correct point where the beam would mostly cover the $200\ \mu\text{m}$ corresponding to the width of an individual cantilever beam.

The laser was oriented through the chosen lens system making sure it would be kept in the chosen horizontal plane and would cross the central portion of the lenses.

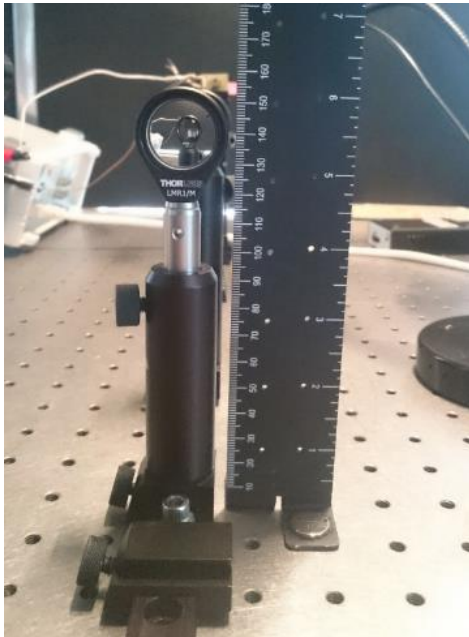


Figure 28: Calibration of lenses height using ruler with scale at 14 cm.



Figure 29: Calibration of laser beam position, so it would cross the central position of each lens.

Due to safety concerns, it would be difficult to verify if the laser spot was precisely pointing to the tip of the cantilever beam. To visually verify and adjust the position of the laser spot, a CCD camera was used in the setup. An extra light source had to be applied to increase the visibility of the cantilever unit so the camera could capture it.

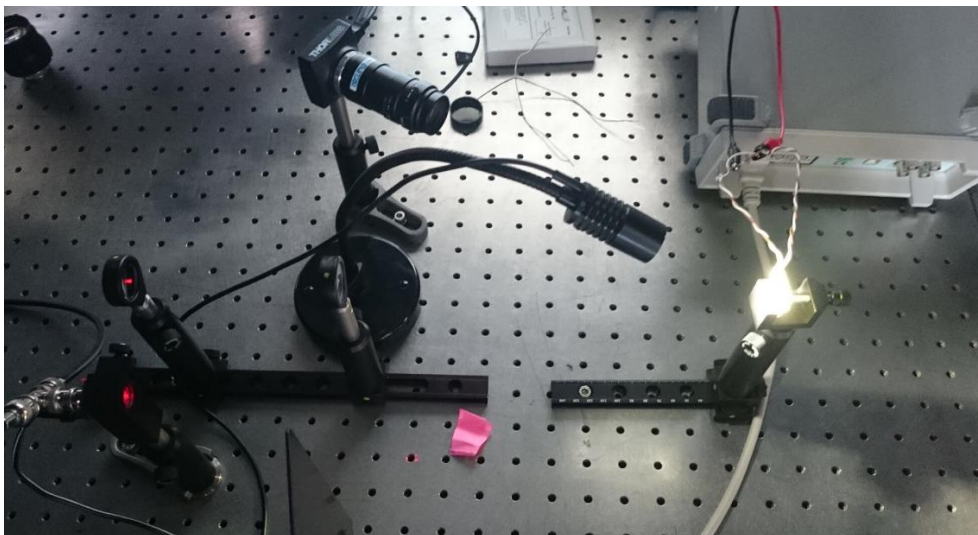


Figure 30: Charge-Coupled Device camera from ThorLabs pointing at cantilever unit (highlighted)

The capture image from the CCD camera can be seen in Figure 31 and Figure 32.

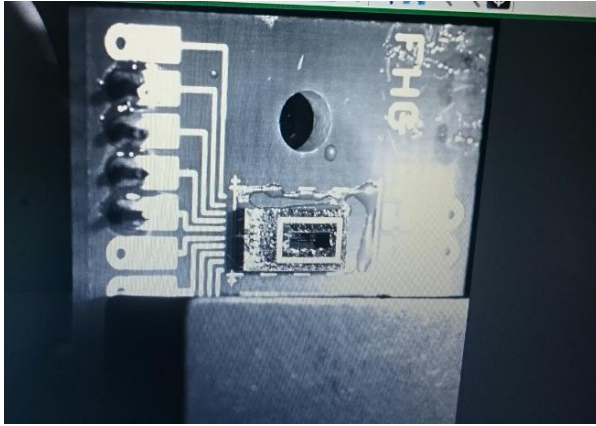


Figure 31: Charge-Coupled Device camera from ThorLabs pointing at cantilever unit (brightly illuminated)

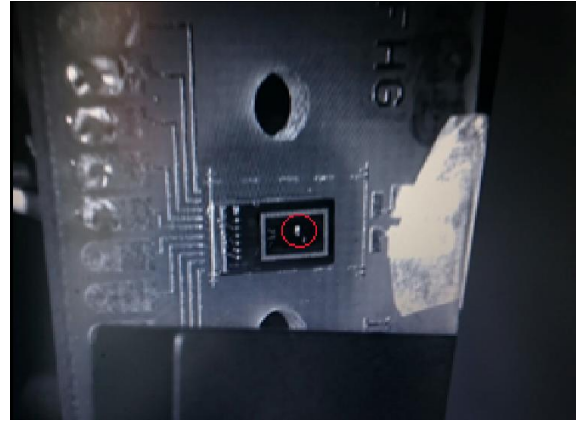


Figure 32: Charge-Coupled Device camera from ThorLabs pointing at cantilever unit with laser spot visible on the end portion of first cantilever beam (highlighted with red circle).

To easily adjust the cantilever unit, its PCB was held on a rail so it could be moved closer to the focusing lenses and turned, allowing for the angle of the reflected light to be adjusted so the beam would be reflected back to the photodiode unit.



Figure 33: Cantilever unit on mounting system

The objective is for the light beam to be reflected to the very edge of the sensitive area of the photodiode unit ($800\text{ }\mu\text{m}$ diameter - see Table 5), so the frequency of the displacement of the light beam can be read. The calculated displacement of the light beam at the chosen distance for the photodiode, as seen in Figure 2 and using equation 5 is just of 105 nm. This is proven to be a challenge since the sensitive area is roughly 7600 times larger and the reflected beam needs to be directed at a very precise point. This adjustment was done by trial and error until a reading signal could be found using the non-functionalized cantilever driven at resonance frequency.

The calibration proved to be a challenge but a weak signal could be read as it is shown in

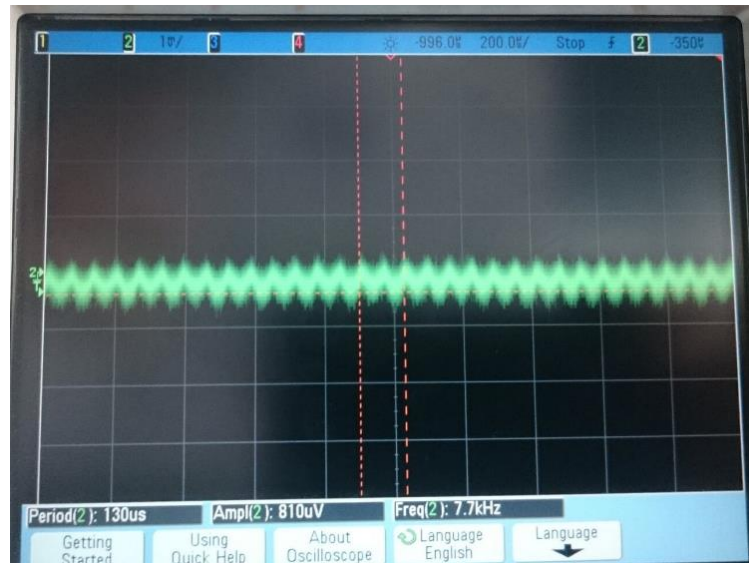


Figure 34: Measured output in a MSO6014A Mixed Signal Oscilloscope from Agilent Technologies

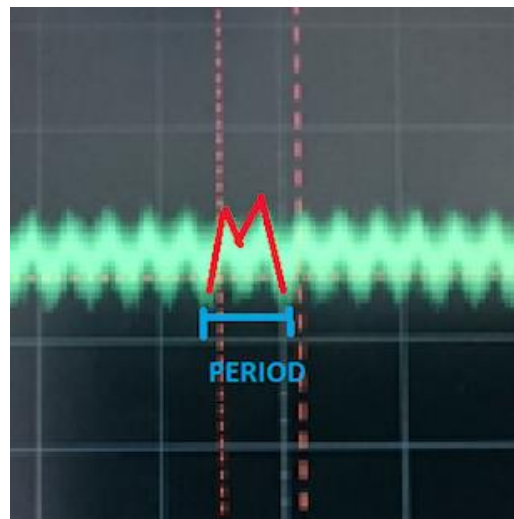


Figure 35: Detail of output with period $T = 130 \text{ uS}$ (each division is of 200 uS)

The signal was quite hard to read and a “M” shaped wave was found with a period of roughly of $130 \mu\text{s}$ which corresponds to an approximate frequency of 7.7 kHz . This gives an error of 1.28% from the original waveform given to the cantilever beam. Again, since it will be shift in frequency that will give the difference in mass (as per equation 4), it was considered an acceptable output for the final tests.

An overall schematic of the optical setup with final distances between components can be seen in Figure 36.

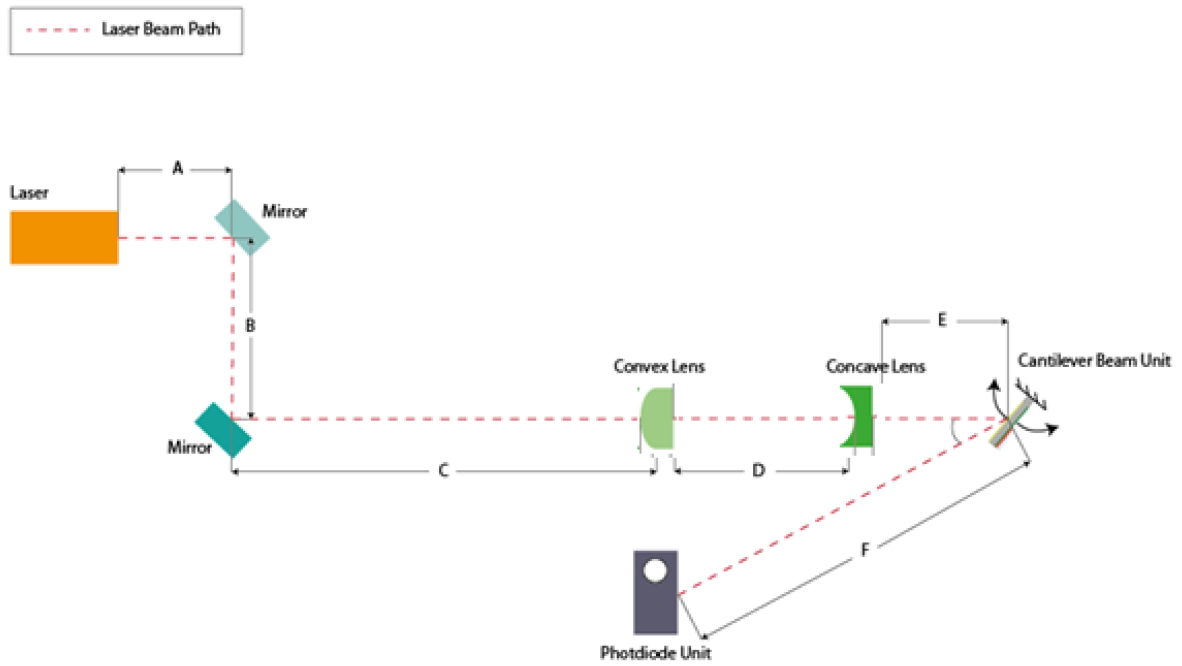


Figure 36: Schematic of components positioning on optical table

Path	A	B	C	D	E	F	Angle of cantilever unit to photodiode
Dimensions (m)	0.11	0.41	1.04	0.17	0.27	40.7	10.6°

Table 10: Measured distances between components placements as seen in Figure 36

Series resonant frequency point Parallel resonant frequency point

Impedance	171 kΩ	175 kΩ
Capacitance	116 pF	112 pF
Frequency	7.92 kHz	7.99 kHz

Table 11: Measurements given by Impedance Analyser

It is noticeable that these values are different than expected when compared with the initial values given by Fraunhofer ISIT. This could be explained by the use of different testing methods. Also it is to be referred that the given data was applicable for generic cantilevers of the same type, and was run at different frequencies. The frequency values also differ but it could be explained by the difference between the mechanical resonant frequency, given by equation 18 and the electrical resonant frequency for RLC circuits is given by equation 19.

$$f = \frac{1}{2\pi} \sqrt{\frac{k}{m}} \quad (13)$$

With k being the spring constant and m, the mass of the mechanical system.

$$f = \frac{1}{2\pi\sqrt{LC}} \quad (14)$$

With L being the inductance and C the capacitance value of the RLC circuit [25].

For simulation purposes the piezo cantilever can be taken as a harmonic oscillator. The recommended electrical equivalent model can be seen in the figure below.

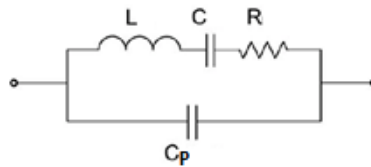


Figure 39: Equivalent model for piezoelectric transducers based on Miyahara et al, McGill University

The value L for the inductance can be calculated using the total capacitance of the system C_{total} and the target frequency f .

$$L = \frac{C_{total}}{(2\pi f)^2} \quad (15)$$

For simulation purposes it is recommended to take $C \ll C_p$ with $C + C_p = C_{total} = C_{measured}$. Based on the measured values at parallel resonant frequency point, a system is designed using NI Multisim 13.5.

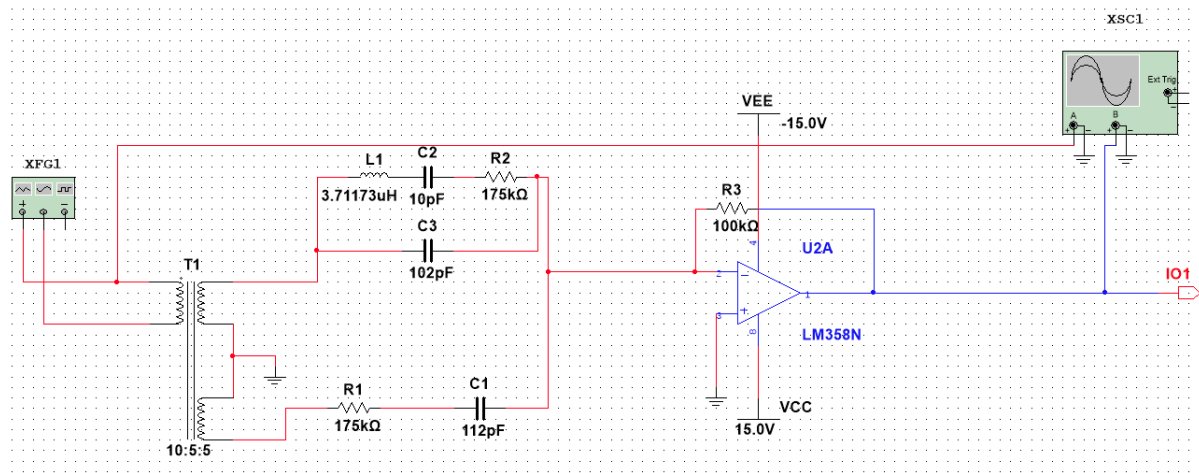


Figure 40: Screen dump from NI Multisim 13.5 with components values

The most approximate values for components were used from the stock already available at the SDU E-Lab. The chosen operational amplifier, the LM358-N is to be used as a transimpedance amplifier since it is easily available and meets the needs for this specific application. A value of $R_3 = 100k\Omega$ was chosen for the negative feedback branch to simplify calculations. The value of R_3 could be increased (to $1M\Omega$, for example) if a bigger sensitivity for the output is needed.

The relation between the measured current change I , and the output voltage V_{out} is given by:

$$V_{out} = -R_3 I \quad (16)$$

The oscilloscope read output from the simulation can be seen in Figure 41.

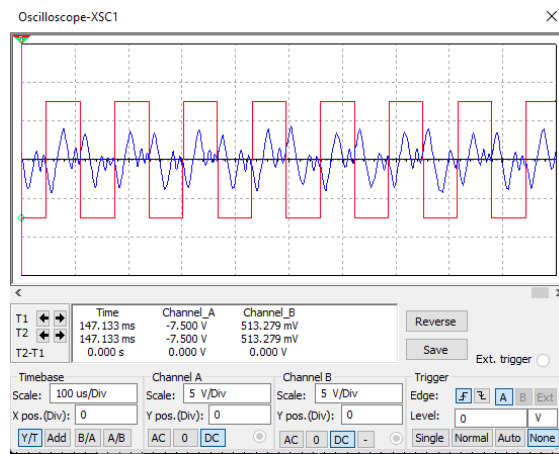


Figure 41: Output from simulation, using virtual oscilloscope. The red line is the given input using a function generator for a square wave of 7.8 kHz and the blue line represents the corresponding output.

By looking at the graph show in Figure 41, the signal (in blue) relates to the natural decay of the resonating cantilever beam after the excitation step.

The only component not ready available at the E-lab in the MCI was the isolation transformer. A more detailed comparison between available models can be found in appendix, section 7.2. The 78250MC Isolation Transformer from Murata was chosen due to its reduced dimensions and current ratings.

Initially a PCB design is made to accommodate trimmed capacitors and resistors to be easily adjustable, however simple testing shows that it can be quite hard to manually adjust precise values for resistance and capacitance. A second design is made to accommodate simple pin insertion components with precise values. The final design and the first and last prototype boards can be seen in the following pictures.

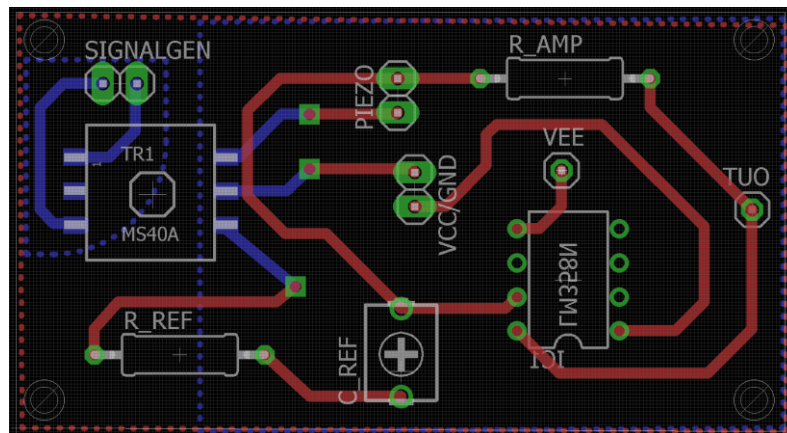


Figure 42: PCB schematic final design using CadSoft EAGLE PCB design 7.5.0 Light

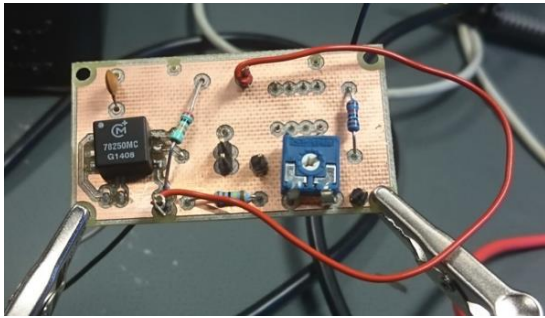


Figure 43: Initial PCB board prototype during tests

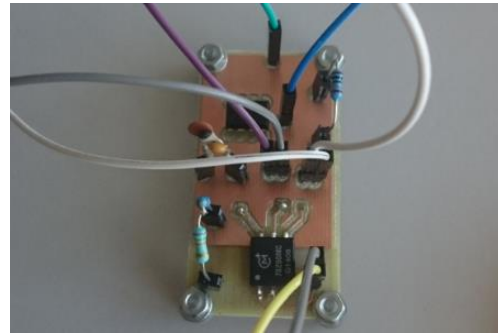


Figure 44: Final PCB board prototype during tests

The final version of the PCB was tested over 1-hour period connected to a MSO6014A Mixed Signal Oscilloscope from Agilent Technologies, connected to the non-functionalized cantilever unit. This model was chosen since it would give on screen statistics over time.

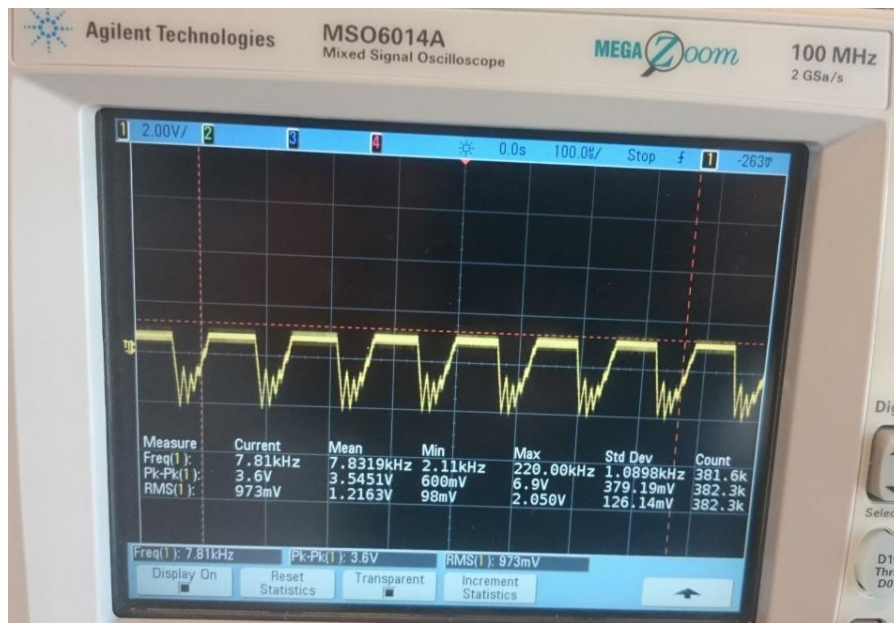


Figure 45: Output from PCB board during 1-hour tests while connected to non-functionalized cantilever with a mean output frequency of 7.832 kHz and standard deviation of 1.090 kHz approximately

It is noticeable that the output is somewhat different than what obtained during the simulation. Still the effect of the expected resonance natural decay of the cantilever is visible after the step input is given. Like previously observed in Figure 21 the behaviour of both piezoelectric layers differ, which might make the simulation an approximation but not accurate enough to describe its full behaviour. For the proposed objectives however it is acceptable, since it will be the shift of measured output voltage and therefore frequency that relates to the mass change of the beam and the amount of captured cadaverine molecules by the functionalized edge of the cantilever

4 Final tests and results

This section describes the final tests performed with a functionalized cantilever unit prepared with cyclam (a cadaverine binding agent) by Fraunhofer ISIT. The cantilever is exposed to cadaverine in increasing longer periods until saturation of the functionalized area is achieved. In a second point the obtained results are presented and discussed.

4.1 Setup description

In previous setups done at the MCI [22] the cantilevers were exposed to a cadaverine solution of water and glycerol, heated up until it reached gas phase. A different test was suggested, using a real-life application for the industry. A piece of chicken breast was carefully prepared, and left for 48 hours inside an air-tight container at ambient temperature. Odour caused by meat degradation should be identifiable by the human nose in just 24 hours after raw meat is left unrefrigerated due to the development of a myriad of potential spoilage bacteria [16]. As previously mentioned this odour is caused by protein hydrolysis, being one of the resultant components cadaverine.



Figure 46: Raw chicken breast after 48 hours exposure to ambient temperature. The odour of spoilage is already felt.

The preparation and exposure of the meat was done under a laboratory fume hood. The PCB containing the functionalized cantilever unit was exposed to close proximity to the meat product. With each exposure the cantilever unit was connected to the Piezo-sensing circuit and the output is measured. Due to the difficulty of calibration of the optical setup, in precisely positioning the cantilever unit so the laser beam would reflect exactly to the edge of the

sensitive area of the photodiode, only two measurements were done. The cantilever was run using an AFG-2125 Arbitrary Function Generator from GW Instek at 7.8 kHz, 10 V_{pp}. The output was read using a MSO6014A Mixed Signal Oscilloscope from Agilent Technologies.



Figure 47: Signal generator setup to drive the piezoelectric beam

The piezo-sensing circuit was placed near the cantilever PCB holder for the optical setup, so testing on both setups would be easier to achieve.

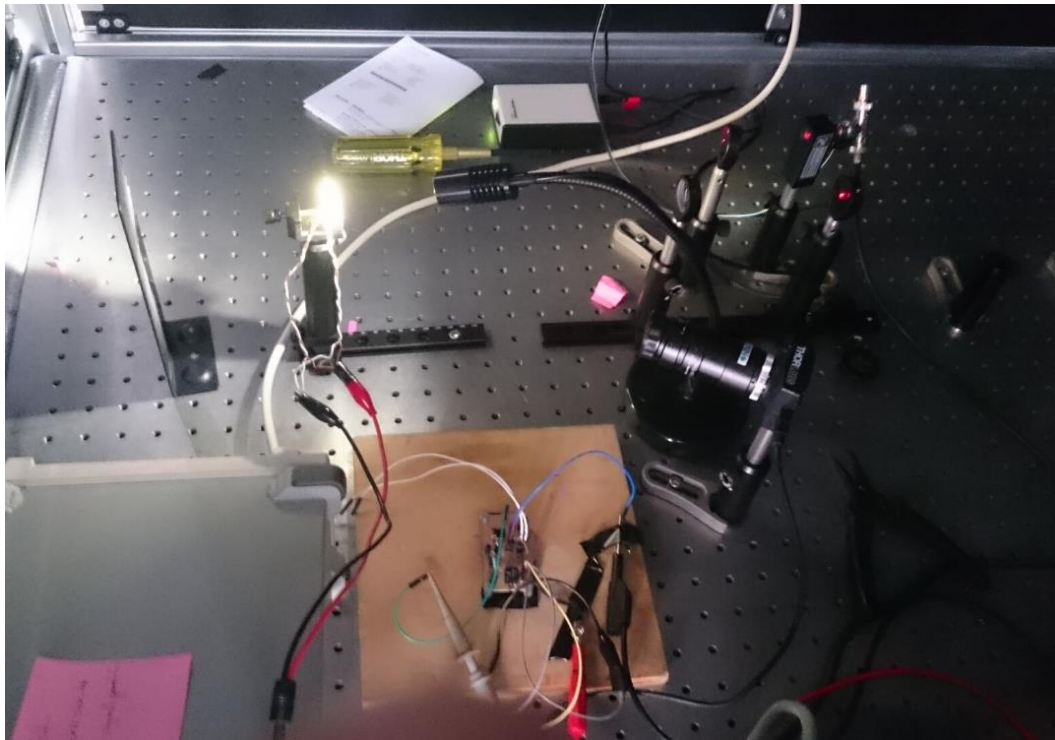


Figure 48: Overview of full testing setup

The results from both setups can be seen in sections 4.2.1 and 4.2.2.

4.2 Results

4.2.1 Piezo sensing circuit

In Table 12 the output results from the piezo-sensing circuit are presented.

<i>Time (s)</i>	<i>Average output voltage (mV)</i>	<i>Calculated current (A)</i>
10	246	0.00246
20	255	0.00255
30	252.8	0.002528
40	269	0.00269
50	267	0.00267
60	273	0.00273
90	290	0.0029
120	291	0.00291
180	289	0.00289

Table 12: Output results read by piezo-sensing circuit and corresponding current using Eq. 20

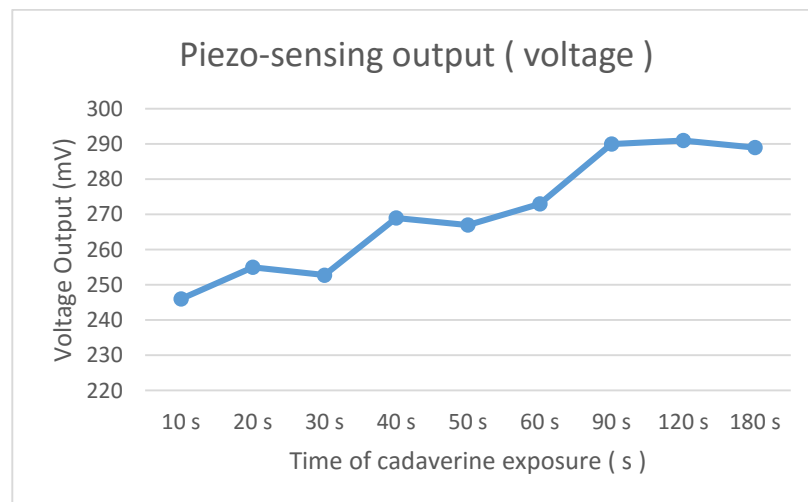


Figure 49: Voltage output vs cadaverine exposure time from the piezo-sensing circuit

As expected the output values should stabilize once the cantilever beam gets saturated with cadaverine molecules. By knowing that for piezoelectric materials the voltage output relates to force applied (compression of piezo crystals). The frequency of operation of a piezoelectric material relates to the current by the following equation [24].

$$f = \frac{I}{2CV_{pp}} \quad (17)$$

Since C, the capacitance is taken as constant for resonating frequency and V_{pp} of the cantilever being driven is also a constant that means that the frequency relates linearly to the output current. However, it was expected that with an increase in mass the current value would be increasingly smaller. Again, since it is the shift of mass that is of interest these values are input into MatLab and calculated accordingly.

<i>Time (s)</i>	<i>Measured mass (kg)</i>
10	1.3247e-07
20	3.3720e-07
30	2.8647e-07
40	6.7082e-07
50	6.2199e-07
60	7.6970e-07
90	1.2088e-06
120	1.2356e-06
180	1.1821e-06

Table 13: Calculated mass change read by piezo-sensing circuit

The obtained values are in the milligrams range. To further analyse this unexpected result a more detail look at the obtained oscilloscope graphic is needed when the circuit is connected to the functionalized cantilever.



Figure 50: Output signal read in oscilloscope for functionalized cantilever chip. It is noted that the behaviour is quite different from the one obtained in previous testing as seen in Figure 45.

By looking at the figure above, it can be seen 2 different periods are recognizable for *Period 1* of about $130\ \mu\text{s}$, a corresponding frequency is of 7.7 kHz, with a rough amplitude of 4V. For *Period 2* it lasts around $25\ \mu\text{s}$. The remaining behaviour of the graphic seems to be caused by the natural decay of the resonance of the cantilever, after receiving its excitation step, but this was expected to happen after the excitation signal stops.

When looking, by comparison, at Figure 45 it can be seen that the corresponding period is quite similar, but the decay is only noted after the excitation step is done.

In section 2.5 it is discussed on how dependent this circuit is of a reference value that correctly mimics the impedance and capacitance values of the cantilever at resonating frequency. A difference in the electrical properties of the piezoelectric layer from the functionalized to the non-functionalized cantilever could explain this unexpected behaviour. A change in environmental conditions, such as temperature could also affect the output [13]. Since this data is unknown in detail for the piezoelectric layer present in the cantilever chips (the effect of hysteresis as an example). As a future consideration an array of cantilevers could be used, both with functionalized and non-functionalized units. The output of both units could be then compared, and zeroed, minimizing the effects of temperature or differences in building process.

4.2.2 Optical setup

As discussed, due to the difficulty in calibrating the piezoelectric unit in the mount of the optical setup, only two measurements were performed, before exposure and after full exposure time. The output in the oscilloscope obtained from the photodiode unit can be seen in the figure below and is present in Table 14.

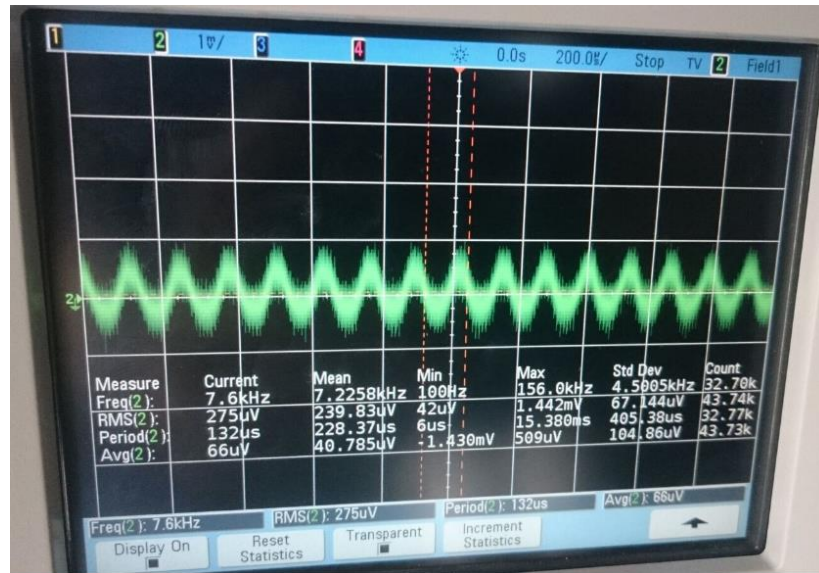


Figure 51: Screenshot of frequency read

	Time (s)	Resulting frequency (Hz)
Before exposure	0	7700
After full exposure	180	7200

Table 14: Output results from optical setup

Below it can be see a simple graphical representation of the found frequency values.

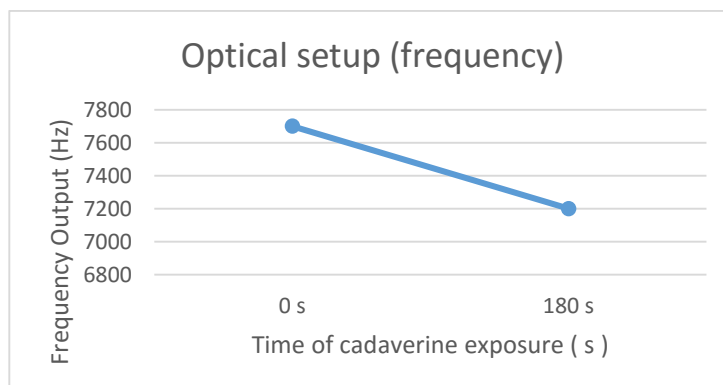


Figure 52: Frequency output vs cadaverine exposure time from the optical setup

Using equation 4, the mass difference is calculated to be of 11.606 picograms (see MatLab script in appendix, section 7.4).

The main challenge of this setup was the difficulty in calibration. Finding the precise point that was needed for the photodiode to be able to read the small deflection changes of the cantilever tip, was quite time consuming. It is of notice that initial signal captured for the non-functionalized cantilever, that served as a reference, could not be read with enough resolution for a mean value to be taken. To increase the movement of the beam at the photodiode level, the distance between the cantilever unit and the sensor could be increased, but this would not be favourable towards the miniaturization process and therefore was discarded.

Building a small casing unit with fixed “click on” positions for the lenses and the cantilever chip, together with the photodiode unit could be a way to minimize issues, by keeping very precise distances and positions on all components. Again like in the previously discussed setup, ideally an array of cantilever units should be used comparing functionalized and non-functionalized units to minimize differences in the building process or environmental factors that could affect the resonant frequency and the obtained output. This would however imply the use of integrated optics on the cantilever beams, which would increase the cost of its microfabrication (as seen in the analysis performed in Table 2).

5 Conclusion

In this section the data obtained from previous studies at the MCI using the AFM method is compared against the 2 developed prototypes and its results. The pertinence of the performed risk assessment is also discussed, and recommendations for further development of this work are highlighted based on the obtained results and faced issues.

5.1 Setups comparison

By looking at the original AFM study done by the MCI with cyclam functionalized cantilevers, these could detect quantities as small as 674 femtograms of cadaverine for a shift of resonance of about 850 Hz. To compare the sensitivity, S , of the different setups it is taken as a simple ratio between the shift of frequency and the shift of mass as it follows:

$$S = \frac{\Delta f}{\Delta m} \quad (18)$$

For easier comparison between the three methods, the chosen values are taken only from the full saturation point of cyclam by cadaverine molecules (180 seconds exposure).

<i>Method</i>	<i>AFM</i>	<i>Optical</i>	<i>Piezo sensing</i>
<i>Sensitivity for saturation point (Hz/Kg)</i>	$\frac{850\text{Hz}}{6.74 \times 10^{-16} \text{ Kg}}$ $= 1.2611 \times 10^{18}$	$\frac{500\text{Hz}}{1.1607 \times 10^{-14} \text{ Kg}}$ $= 4.3079 \times 10^{16}$	$\frac{192\text{Hz}}{1.1821 \times 10^{-06} \text{ Kg}}$ $= 1.6243 \times 10^8$

Table 15: Sensitivity comparison between the three methods in Hz/Kg.

It can be seen that regarding sensitivity the AFM and Optical setups the most similar. However, it has to be noted that no mean measurement could be achieved for the optical setup for its reference value, it was visually calculated by observation of the oscilloscope graphical output. It is also of notice that the dimensions and resonance frequencies of the cantilever beam used in the AFM setup were quite different (smaller dimensions' cantilever, with resonance at much higher frequency), which can of course influence the final results. Although promising, the values obtained by the Optical setup would have to be validated by repeated experiments, while achieving saturation curves and comparing deviation between each experimental measurement.

By looking at the piezo sensing values, although it is not possible to confirm at this moment the amount of cadaverine effectively captured by the functionalized area of the cantilever, a

result of captured cadaverine mass in the milligrams range for a functionalized length of only 100 μm seems off. It was also noticed that there should have been a decrease in voltage rather than the observed increasing values, since a decrease in frequency due to the increasing mass was the expected result. Unfortunately, it was not possible to run this test setup again, since only a single unit of the functionalized cantilever chip was obtained. Some of the possibilities for the failure of this setup were discussed previously in section 4.2.1.

The three setups are then compared for the overall cost, together with possible minimization possibilities, for everyday professional side by side against already existing methods like Gas Chromatography.

<i>Method</i>	<i>AFM</i>	<i>Optical</i>	<i>Piezo sensing</i>
<i>Overall cost</i> <i>(Qualitative)</i>	High cost	Medium cost	Low cost
<i>Minimization</i> <i>possibility</i>	Low	Medium	High

Table 16: Cost and minimization comparison between the three methods.

All the methods described above have in common the cost of the functionalized cantilever chip on PCB, which for these research and development units is about 30 DKK. However according to Fraunhofer ISIT the optimized production price could go down to 7.44 DKK.

Gas chromatographs (GCMS) costs can go around 400000 DKK (Shimadzu). For AFM the cheapest kit found starts at 210000 DKK (AFM Workshop) making it still a quite expensive technology, with simple parts like the probe system costing around 8000 DKK per unit.

For the optical setup and looking at a possible miniaturization and improvements, the main costs would be a laser diode unit together with the lenses system and photodiode unit. By looking at the components available from ThorLabs, the total cost for these would be of 5600 DKK.

Finally, the piezo sensing unit would be the cheapest and smallest of all the solutions described previously. It requires just a few electronic components and PCB manufacturing, making a total cost of 430 DKK. However, it is of notice that this unit did not perform as expected and further development would be needed on it, with the possible implementation of

band pass filtering and closed loop control, which would increase its final cost, excluding the man hours of extra development.

Going a bit further by looking at full portability for a finished commercially available device, both the piezo sensing and optical setups would need a microcontroller unit to read its output and display them to the user, which would also increase their costs, but not significantly when compared to the AFM and GCMS options.

Accuracy could not be objectively compared since it was not possible to measure the real amount of cadaverine trapped by the functionalized area of the cantilever. Cantilevers with different dimensions were used in the work of *Wang et al* [22], for the AFM setup made at the MCI. For calculation and simulation purposes it was assumed that the functionalized area would still cause a mass shift of 674 femtograms, and the results from the AFM setup as being fully accurate.

<i>Method</i>	<i>Optical</i>	<i>Piezo sensing</i>
<i>Accuracy</i>	Higher	Smaller

Table 17: Qualitative accuracy comparison between the different methods, by taking the smallest difference to the mass found in the AFM.

Overall, and considering the obtained data it is then thought that the optical setup shows the best promises of a future product.

5.2 Risk assessment

Several risks were met during the development of this project, these can be seen highlighted in the figure below The full version of the risk assessment can be found in appendix, section 7.5.

Seq. No.	Category	Description of risk	Trigger point of risk	Effect on the project	Impact	Probability in %	Risk Level
1	Mechanical	Direct physical damage to parts	Assembly of prototype	Assembly delay, additional costs	5	60%	3.0
2	Mechanical	Piezocantilever sensitivity not adequate	Assembly of prototype	Requirements not met	5	20%	1.0
3	Mechanical	Production/Acquisition of parts too expensive	Designing	Not able to use anticipated parts	4	60%	2.0
4	Mechanical	Cantilever and piezo not easily assembled	Assembly of prototype	Requirements not met	4	60%	2.0
5	Mechanical	Laser displacement not adequate for photodiode detector	Test of electronics and optics	More time needed, additional cost	2	40%	1.0
6	Electrical	Acquisition of parts too expensive	Designing	Not able to use anticipated parts	5	40%	2.0
7	Electrical	Parts damaged	Test of electronics and optics	More time needed, additional cost	5	60%	3.0
8	Electrical	Circuit not working as intended	Test of electronics and optics	More time needed	2	60%	2.0
9	Electrical	Laser related injury	Assembly of prototype	Temporary or permanent injury	5	20%	1.0
10	Electrical	Electric components not compatible	Test of electronics and optics	More time needed, additional cost	5	40%	2.0
11	Electrical	Noise from unwanted sources	Test of electronics and optics	More time needed	4	60%	2.0
12	Electrical	Risk of electrocution	Assembly of prototype	Temporary or permanent injury	5	20%	1.0
13	Production	Electric components late failure	Integration tests	More time needed, additional cost	4	40%	2.0
14	Production	Final product not behaving according to simulations/expectations	Integration tests	Risk of requirements not met/Further research needed	5	40%	2.0
15	Production	Final product not able to give any output for comparison requirements	Integration tests	Requirements not met	5	40%	2.0
16	Marketing	Final product not meeting market / Proposed requirements for portability	Final review	Requirements not met	5	40%	2.0

Figure 53: Caption or risk assessment table with encountered risks highlighted in green

These had impact in the project development, causing delays in the workflow. and mostly are already discussed in their corresponding sections.

One that still remains to be discussed is regarding the damaged on-chip cantilever beams that are extremely fragile, and not easily repairable. Two non-functionalized units were damaged during simple postal transport and during manipulation for tests procedures as it can be seen in Figure 54.

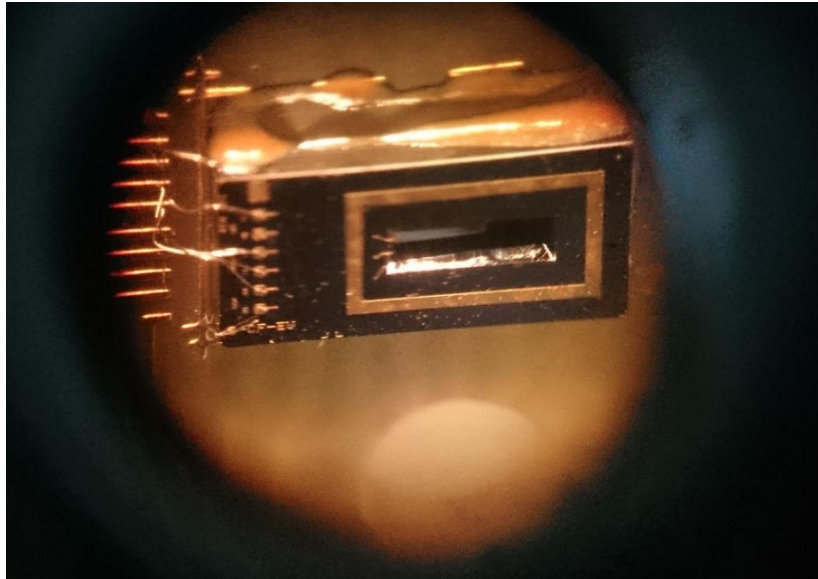


Figure 54: Zoomed image of damaged cantilever chip, with bent beam and connectors broken.

Better care on transport should be taken into care, by firmly fixing the PCB with the chip to the protective case. Also manipulation of these units should be minimized, since they should be considered as single-use (as it would be in a mass production prototype). It is desirable for the units to be easily replaceable, without affecting calibration of the device.

This single risk was what most affected the time plan of the project, since tests had to be postponed until new units were obtained. In total 3 units were used for tests. It was accordingly identified in the risk assessment with the highest risk level.

Therefore, in future tests it should be considered to have a fair amount of units at disposal during the test procedures.

5.3 Final considerations

For a future product, it is advisable to use a standardized cantilever unit, built for the specific application of in a piezo-sensing circuit or optical setup with well-known mechanical and electrical properties.

The optical properties of the silicon cantilever could also be improved, since these units were not gold coated on its surface, affecting the reflection of the laser beam. This would allow for better quality simulations and planning of a working setup.

As a reference value the same cantilever types should be tested under AFM, to determine the amount of cadaverine molecules binding to the

Finally, and specifically for the optical setup a closed casing should be considered where the exact position of lenses and the cantilever unit are defined, avoiding calibration issues. The use of a quadrant-photodiode could also help the miniaturization process, since it would be more adequate to detect such small displacements of the laser beam caused by the shift in resonance frequency, shortening the needed distance between the cantilever and the detector.

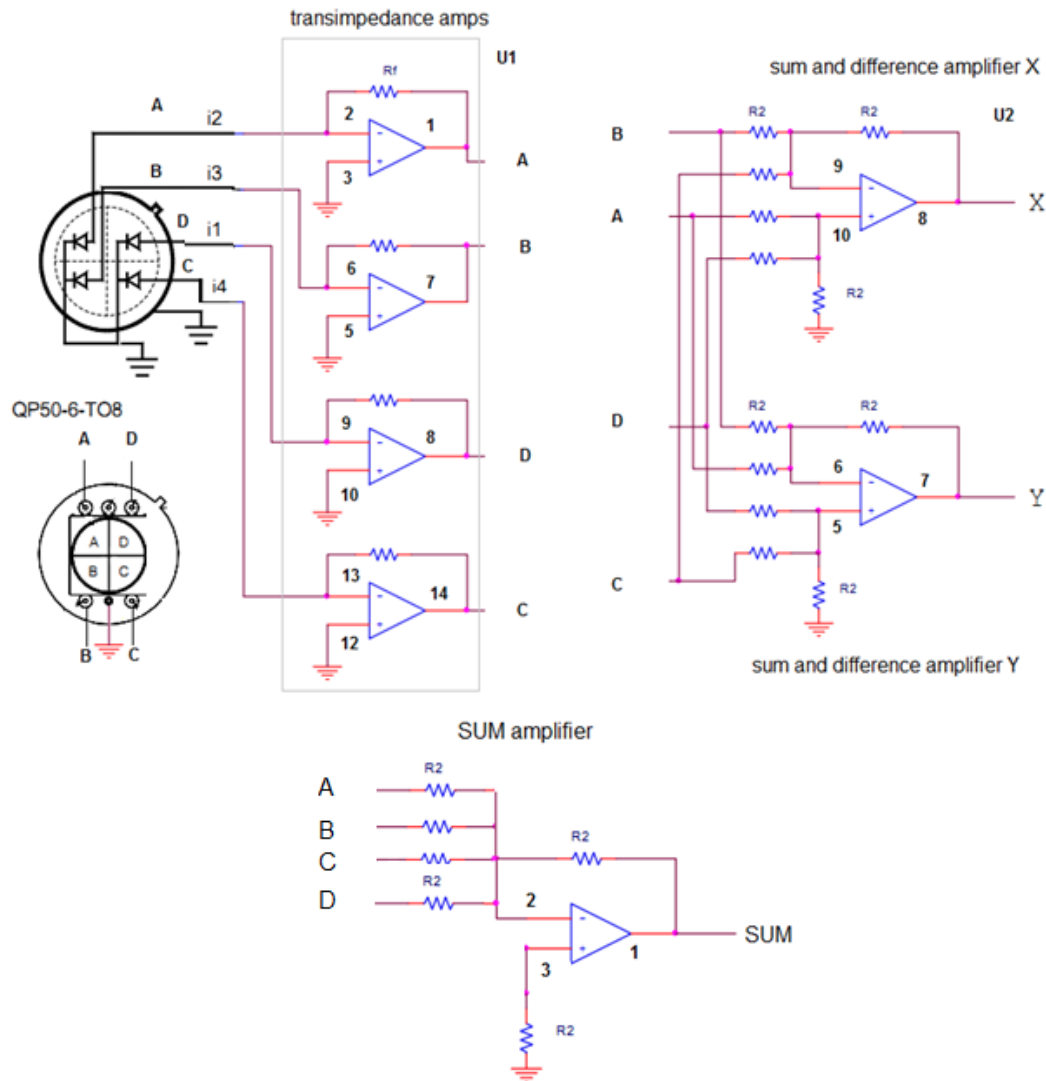
6 References

- [1] Alvarez, M. and Lechuga, L. (2010). Microcantilever-based platforms as biosensing tools. *The Analyst*, 135(5), p.827.
- [2] Boisen, A., Dohn, S., Keller, S., Schmid, S. and Tenje, M. (2011). Cantilever-like micromechanical sensors. *Rep. Prog. Phys.*, 74(3), p.036101.
- [3] Cdc.gov. (2016). *Healthcare-associated infections | HAI | CDC*. [online] Available at: <http://www.cdc.gov/HAI/> [Accessed 30 May 2016].
- [4] *Curriculum Chapter 9, BSc (Eng) in Engineering (Mechatronics), Study start September 2012, Version 1.0 – Syddansk Universitet, Sønderborg*
- [5] Elisa-antibody.com. (2016). *ELISA for Food Industry*. [online] Available at: <http://www.elisa-antibody.com/applications/food-industry> [Accessed 30 May 2016].
- [6] Evtugyn, G (2014) *Biosensors: Essentials*. Berlin, Heidelberg: Springer Berlin Heidelberg.
- [7] Feng, X., Huang, Y. and Rosakis, A. (2007). On the Stoney Formula for a Thin Film/Substrate System With Nonuniform Substrate Thickness. *Journal of Applied Mechanics*, 74(6), p.1276.
- [8] Gere, J. and Timoshenko, S. (1997). *Mechanics of materials*. Boston: PWS Pub Co.
- [9] Hatch, M. (2001). *Vibration simulation using MATLAB and ANSYS*. Boca Raton: Chapman & Hall/CRC.
- [10] HeNe gas lasers vs. laser diode modules. (2004). 1st ed. [ebook] Little Rock: Power Technology Incorporated, p.1. Available at: http://www.photoniccomponentgroup.com/PDFs/WP_HeNe-vs-diodelaser.pdf [Accessed 30 May 2016].
- [11] Memsnet.org. (2016). *MEMS and Nanotechnology Applications*. [online] Available at: <https://www.memsnet.org/mems/applications.html> [Accessed 30 May 2016].
- [12] Miyahara, Y., Deschler, M., Fujii, T., Watanabe, S. and Bleuler, H. (2002). Non-contact atomic force microscope with a PZT cantilever used for deflection sensing, direct oscillation and feedback actuation. *Applied Surface Science*, 188(3-4), pp.450-455.
- [13] Morita, S., Giessibl, F., Meyer, E. and Wiesendanger, R. (n.d.). *Noncontact atomic force microscopy*.
- [14] Naila, A., Flint, S., Fletcher, G., Bremer, P. and Meerdink, G. (2010). Control of Biogenic Amines in Food-Existing and Emerging Approaches. *Journal of Food Science*, 75(7), pp.R139-R150.
- [15] Pedrotti, F., Pedrotti, L. and Pedrotti, L. (2007). *Introduction to optics*. Upper Saddle River, N.J.: Pearson Prentice Hall.
- [16] Ray, B. and Bhunia, A. (2013). *Fundamental Food Microbiology, Fifth Edition*. Hoboken: CRC Press.
- [17] Repairfaq.org. (2016). *necbr1-1*. [online] Available at: <http://www.repairfaq.org/sam/brochures/NECBR1988/necbr11.html> [Accessed 30 May 2016].

- [18] Rijk, I. (2016). *Design of a Metrological Atomic Force Microscope Head*. Master. Technische Universiteit Eindhoven.
- [19] Saleh, B. and Teich, M. (2007). *Fundamentals of photonics*. Hoboken, N.J.: Wiley-Interscience.
- [20] Stone, P. (2009). Economic burden of healthcare-associated infections: an American perspective. *Expert Review of Pharmacoeconomics & Outcomes Research*, 9(5), pp.417-422.
- [21] Waggoner, P. and Craighead, H. (2007). Micro- and nanomechanical sensors for environmental, chemical, and biological detection. *Lab on a Chip*, 7(10), p.1238.
- [22] Wang, Y. et al (2015). Functionalizing micro-cantilevers for meat degradation measurements. p.8.
- [23] Wikipedia. (2016). *Lens (optics)*. [online] Available at: [https://en.wikipedia.org/wiki/Lens_\(optics\)](https://en.wikipedia.org/wiki/Lens_(optics)) [Accessed 30 May 2016].
- [24] Piezo.ws. (2016). *Piezo Mechanics Design Tutorial: Piezoelectricity, Forces and Stiffness ;* &. [online] Available at: http://www.piezo.ws/piezoelectric_actuator_tutorial/Piezo_Design_part3.php [Accessed 30 May 2016].
- [25] Efunda.com. (2016). *eFunda: Equivalent Circuit of Piezo Materials*. [online] Available at: http://www.efunda.com/materials/piezo/electronics/elec_equiv_circuit.cfm [Accessed 30 May 2016].

7 Appendices

7.1 Quadrant photodiode recommended circuit



Marett, D. (2016). *A four quadrant photodetector for measuring laser pointing stability*.
[online] Conspiracyoflight.com. Available at:
<http://www.conspiracyoflight.com/Quadrant/Quadrant.html> [Accessed 30 May 2016].

7.2 Comparison of Isolation transformers

<i>Manufacturer and Model</i>	<i>Murata Power Solutions 78250MC</i>	<i>Murata Power Solutions 78250VC</i>	<i>Murata Power Solutions 1605C</i>	<i>Murata Power Solutions 78253JC</i>
<i>Max Input current</i>	300mA	300mA	n/a	100mA
<i>Isolation voltage limit</i>	1.4kVrms	4.0kVrms	500Vrms	1.5kVrms
<i>Turn ratio</i>	1:1	1:1	1:1	1:1.31
<i>Dimensions (mm)</i>	6.35x9.52x9	6.35x9.52x9	5.8x22.5x6.86	6.35x12.7x9
<i>Pin mounting</i>	SMD	Through hole	Through hole	SMD

Murata-ps.com. (2016). *Murata Power Solutions | DC-DC Converter, AC-DC Power Supply, Digital Panel Meter, Inductor, Common Mode Choke and Pulse Transformer | Murata Power Solutions*. [online] Available at: <http://www.murata-ps.com/> [Accessed 30 May 2016].

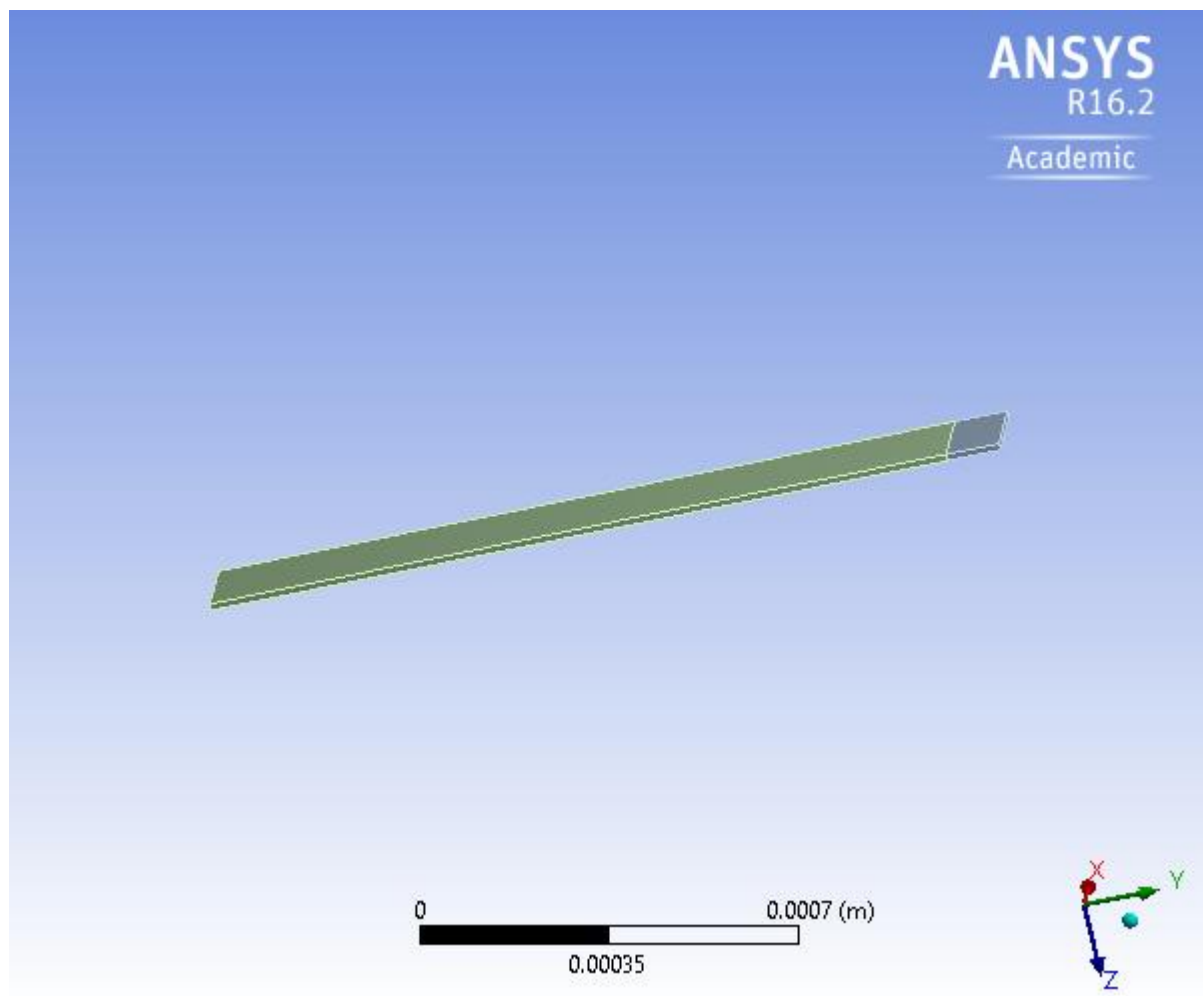
7.3 Beam resonance in ANSYS

INITIAL STATE



Project

First Saved	Tuesday, February 23, 2016
Last Saved	Tuesday, May 31, 2016
Product Version	16.2 Release
Save Project Before Solution	No
Save Project After Solution	No



Contents

- [Units](#)
- [Model \(B4\)](#)
 - [Geometry](#)
 - [Parts](#)
 - [Coordinate Systems](#)
 - [Connections](#)
 - [Contacts](#)
 - [Contact Region](#)
 - [Mesh](#)
 - [Modal \(B5\)](#)
 - [Pre-Stress \(None\)](#)
 - [Analysis Settings](#)
 - [Fixed Support 2](#)
 - [Solution \(B6\)](#)
 - [Solution Information](#)
 - [Results](#)
- [Material Data](#)
 - [Si - Au Cantilever](#)

Units

TABLE 1

Unit System	Metric (m, kg, N, s, V, A) Degrees rad/s Celsius
Angle	Degrees
Rotational Velocity	rad/s
Temperature	Celsius

Model (B4)

Geometry

TABLE 2
Model (B4) > Geometry

Object Name	Geometry
State	Fully Defined
Definition	
Source	F:\Dropbox\BSc Mechatronics - SDU\Classes\6 MC\Thesis\ANSYS\cantilever_3_files\dp0\SYS-1\DM\SYS-1.agdb
Type	DesignModeler
Length Unit	Micrometers
Element Control	Program Controlled
Display Style	Body Color
Bounding Box	
Length X	2.e-004 m
Length Y	1.5e-003 m
Length Z	1.25e-005 m
Properties	
Volume	3.75e-012 m ³
Mass	8.7738e-011 kg

Scale Factor Value	1.
Statistics	
Bodies	2
Active Bodies	2
Nodes	5281
Elements	690
Mesh Metric	None
Basic Geometry Options	
Parameters	Yes
Parameter Key	DS
Attributes	No
Named Selections	No
Material Properties	No
Advanced Geometry Options	
Use Associativity	Yes
Coordinate Systems	No
Reader Mode Saves Updated File	No
Use Instances	Yes
Smart CAD Update	No
Compare Parts On Update	No
Attach File Via Temp File	Yes
Temporary Directory	C:\Users\Carlos\AppData\Roaming\Ansys\v162
Analysis Type	3-D
Decompose Disjoint Geometry	Yes
Enclosure and Symmetry Processing	Yes

TABLE 3
Model (B4) > Geometry > Parts

Object Name	Solid		Solid	
State	Meshed			
Graphics Properties				
Visible	Yes			
Transparency	1			
Definition				
Suppressed	No			
Stiffness Behavior	Flexible			
Coordinate System	Default Coordinate System			
Reference Temperature	By Environment			
Material				
Assignment	Si - Au Cantilever			
Nonlinear Effects	Yes			
Thermal Strain Effects	Yes			
Bounding Box				
Length X	2.e-004 m			
Length Y	1.e-004 m		1.4e-003 m	
Length Z	1.25e-005 m			
Properties				
Volume	2.5e-013 m³		3.5e-012 m³	

Mass	5.8492e-012 kg	8.1888e-011 kg
Centroid X	1.e-004 m	
Centroid Y	1.45e-003 m	7.e-004 m
Centroid Z	6.25e-006 m	
Moment of Inertia Ip1	4.9505e-021 kg·m ²	1.3376e-017 kg·m ²
Moment of Inertia Ip2	1.9573e-020 kg·m ²	2.7403e-019 kg·m ²
Moment of Inertia Ip3	2.4372e-020 kg·m ²	1.3648e-017 kg·m ²
Statistics		
Nodes	428	4853
Elements	50	640
Mesh Metric	None	

Coordinate Systems

TABLE 4
Model (B4) > Coordinate Systems > Coordinate System

Object Name	<i>Global Coordinate System</i>
State	Fully Defined
Definition	
Type	Cartesian
Coordinate System ID	0.
Origin	
Origin X	0. m
Origin Y	0. m
Origin Z	0. m
Directional Vectors	
X Axis Data	[1. 0. 0.]
Y Axis Data	[0. 1. 0.]
Z Axis Data	[0. 0. 1.]

Connections

TABLE 5
Model (B4) > Connections

Object Name	<i>Connections</i>
State	Fully Defined
Auto Detection	
Generate Automatic Connection On Refresh	Yes
Transparency	
Enabled	Yes

TABLE 6
Model (B4) > Connections > Contacts

Object Name	<i>Contacts</i>
State	Fully Defined
Definition	
Connection Type	Contact
Scope	
Scoping Method	Geometry Selection
Geometry	All Bodies
Auto Detection	
Tolerance Type	Slider

Tolerance Slider	0.
Tolerance Value	3.7833e-006 m
Use Range	No
Face/Face	Yes
Face/Edge	No
Edge/Edge	No
Priority	Include All
Group By	Bodies
Search Across	Bodies
Statistics	
Connections	1
Active Connections	1

TABLE 7
Model (B4) > Connections > Contacts > Contact Regions

Object Name	<i>Contact Region</i>
State	Fully Defined
Scope	
Scoping Method	Geometry Selection
Contact	1 Face
Target	1 Face
Contact Bodies	Solid
Target Bodies	Solid
Definition	
Type	Bonded
Scope Mode	Automatic
Behavior	Program Controlled
Trim Contact	Program Controlled
Trim Tolerance	3.7833e-006 m
Suppressed	No
Advanced	
Formulation	Program Controlled
Detection Method	Program Controlled
Penetration Tolerance	Program Controlled
Elastic Slip Tolerance	Program Controlled
Normal Stiffness	Program Controlled
Update Stiffness	Program Controlled
Pinball Region	Program Controlled
Geometric Modification	
Contact Geometry Correction	None
Target Geometry Correction	None

Mesh

TABLE 8
Model (B4) > Mesh

Object Name	<i>Mesh</i>
State	Solved
Display	
Display Style	Body Color
Defaults	
Physics Preference	Mechanical

Relevance	0
Sizing	
Use Advanced Size Function	Off
Relevance Center	Fine
Element Size	Default
Initial Size Seed	Active Assembly
Smoothing	Medium
Transition	Fast
Span Angle Center	Coarse
Minimum Edge Length	1.25e-005 m
Inflation	
Use Automatic Inflation	None
Inflation Option	Smooth Transition
Transition Ratio	0.272
Maximum Layers	5
Growth Rate	1.2
Inflation Algorithm	Pre
View Advanced Options	No
Patch Conforming Options	
Triangle Surface Mesher	Program Controlled
Patch Independent Options	
Topology Checking	No
Advanced	
Number of CPUs for Parallel Part Meshing	Program Controlled
Shape Checking	Standard Mechanical
Element Midside Nodes	Program Controlled
Straight Sided Elements	No
Number of Retries	Default (4)
Extra Retries For Assembly	Yes
Rigid Body Behavior	Dimensionally Reduced
Mesh Morphing	Disabled
Defeaturing	
Pinch Tolerance	Please Define
Generate Pinch on Refresh	No
Automatic Mesh Based Defeaturing	On
Defeaturing Tolerance	Default
Statistics	
Nodes	5281
Elements	690
Mesh Metric	None

Modal (B5)

TABLE 9
Model (B4) > Analysis

Object Name	<i>Modal (B5)</i>
State	Solved
Definition	
Physics Type	Structural
Analysis Type	Modal
Solver Target	Mechanical APDL
Options	

Environment Temperature	22. °C
Generate Input Only	No

TABLE 10
Model (B4) > Modal (B5) > Initial Condition

Object Name	<i>Pre-Stress (None)</i>
State	Fully Defined
Definition	
Pre-Stress Environment	None

TABLE 11
Model (B4) > Modal (B5) > Analysis Settings

Object Name	<i>Analysis Settings</i>
State	Fully Defined
Options	
Max Modes to Find	2
Limit Search to Range	No
Solver Controls	
Damped	Yes
Solver Type	Program Controlled
Rotordynamics Controls	
Coriolis Effect	Off
Campbell Diagram	Off
Output Controls	
Stress	No
Strain	No
Nodal Forces	No
Calculate Reactions	No
General Miscellaneous	No
Damping Controls	
Stiffness Coefficient Define By	Direct Input
Stiffness Coefficient	0.
Mass Coefficient	0.
Analysis Data Management	
Solver Files Directory	F:\Dropbox\BSc Mechatronics - SDU\Classes\6 MC\Thesis\ANSYS\cantilever_3_files\dp0\SYS-4\MECH\
Future Analysis	None
Scratch Solver Files Directory	
Save MAPDL db	No
Delete Unneeded Files	Yes
Solver Units	Active System
Solver Unit System	mks

TABLE 12
Model (B4) > Modal (B5) > Loads

Object Name	<i>Fixed Support 2</i>
State	Fully Defined
Scope	
Scoping Method	Geometry Selection

Geometry	1 Face
Definition	
Type	Fixed Support
Suppressed	No

Solution (B6)

TABLE 13
Model (B4) > Modal (B5) > Solution

Object Name	<i>Solution (B6)</i>
State	Solved
Adaptive Mesh Refinement	
Max Refinement Loops	1.
Refinement Depth	2.
Information	
Status	Done
Post Processing	
Calculate Beam Section Results	No

The following bar chart indicates the frequency at each calculated mode.

FIGURE 1
Model (B4) > Modal (B5) > Solution (B6)



TABLE 14
Model (B4) > Modal (B5) > Solution (B6)

Mode	Damped Frequency [Hz]	Stability [Hz]	Modal Damping Ratio	Logarithmic Decrement
1.	76971	0.	0.	0.
2.	4.8233e+005			

TABLE 15
Model (B4) > Modal (B5) > Solution (B6) > Solution Information

Object Name	<i>Solution Information</i>
State	Solved
Solution Information	
Solution Output	Solver Output
Newton-Raphson Residuals	0
Update Interval	2.5 s
Display Points	All
FE Connection Visibility	
Activate Visibility	Yes
Display	All FE Connectors
Draw Connections Attached To	All Nodes
Line Color	Connection Type
Visible on Results	No
Line Thickness	Single
Display Type	Lines

TABLE 16
Model (B4) > Modal (B5) > Solution (B6) > Results

Object Name	Total Deformation Mode 1		Total Deformation Mode 2
State	Solved		
Scope			
Scoping Method	Geometry Selection		
Geometry	All Bodies		
Definition			
Type	Total Deformation		
Mode	1.	2.	
Sweeping Phase	0. °		
Identifier			
Suppressed	No		
Results			
Minimum	0. m		
Maximum	2.1382e+005 m	2.1377e+005 m	
Minimum Occurs On	Solid		
Maximum Occurs On	Solid		
Information			
Damped Frequency	76971 Hz	4.8233e+005 Hz	
Stability	0. Hz		
Modal Damping Ratio	0.		
Logarithmic Decrement	0.		

TABLE 17
Model (B4) > Modal (B5) > Solution (B6) > Total Deformation Mode 1

Mode	Damped Frequency [Hz]	Stability [Hz]	Modal Damping Ratio	Logarithmic Decrement
1.	76971	0.	0.	0.
2.	4.8233e+005			

TABLE 18
Model (B4) > Modal (B5) > Solution (B6) > Total Deformation Mode 2

Mode	Damped Frequency [Hz]	Stability [Hz]	Modal Damping Ratio	Logarithmic Decrement
1.	76971	0.	0.	0.
2.	4.8233e+005			

Material Data

Si - Au Cantilever

TABLE 19
Si - Au Cantilever > Constants

Density	23.397 kg m ⁻³
---------	---------------------------

TABLE 20
Si - Au Cantilever > Isotropic Elasticity

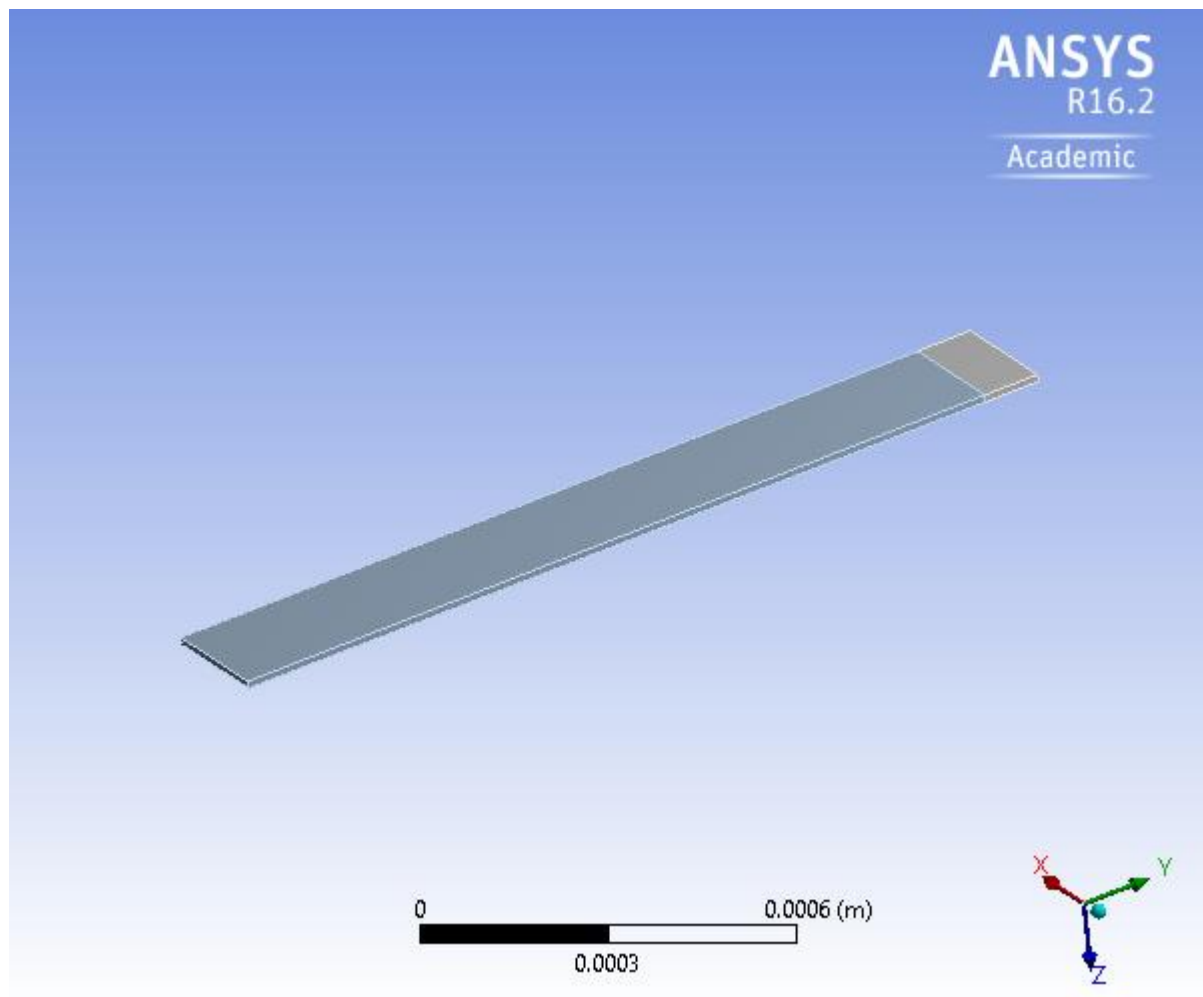
Temperature C	Young's Modulus Pa	Poisson's Ratio	Bulk Modulus Pa	Shear Modulus Pa
	1.7e+011	0.24	1.0897e+011	6.8548e+010

FINAL STATE



Project

First Saved	Sunday, May 22, 2016
Last Saved	Tuesday, May 31, 2016
Product Version	16.2 Release
Save Project Before Solution	No
Save Project After Solution	No



Contents

- [Units](#)
- [Model \(C4\)](#)
 - [Geometry](#)
 - [Parts](#)
 - [Coordinate Systems](#)
 - [Connections](#)
 - [Contacts](#)
 - [Contact Region](#)
 - [Mesh](#)
 - [Modal \(C5\)](#)
 - [Pre-Stress \(None\)](#)
 - [Analysis Settings](#)
 - [Fixed Support](#)
 - [Solution \(C6\)](#)
 - [Solution Information](#)
 - [Results](#)
- [Material Data](#)
 - [Si-Au mass change](#)
 - [Si - Au Cantilever](#)

Units

TABLE 1

Unit System	Metric (m, kg, N, s, V, A) Degrees rad/s Celsius
Angle	Degrees
Rotational Velocity	rad/s
Temperature	Celsius

Model (C4)

Geometry

TABLE 2
Model (C4) > Geometry

Object Name	<i>Geometry</i>
State	Fully Defined
Definition	
Source	F:\Dropbox\BSc Mechatronics - SDU\Classes\6 MC\Thesis\ANSYS\cantilever_3_files\dp0\SYS-1\DM\SYS-1.agdb
Type	DesignModeler
Length Unit	Micrometers
Element Control	Program Controlled
Display Style	Body Color
Bounding Box	
Length X	2.e-004 m
Length Y	1.5e-003 m
Length Z	1.25e-005 m
Properties	
Volume	3.75e-012 m ³

Mass	8.774e-011 kg
Scale Factor Value	1.
Statistics	
Bodies	2
Active Bodies	2
Nodes	5281
Elements	690
Mesh Metric	None
Basic Geometry Options	
Parameters	Yes
Parameter Key	DS
Attributes	No
Named Selections	No
Material Properties	No
Advanced Geometry Options	
Use Associativity	Yes
Coordinate Systems	No
Reader Mode Saves Updated File	No
Use Instances	Yes
Smart CAD Update	No
Compare Parts On Update	No
Attach File Via Temp File	Yes
Temporary Directory	C:\Users\Carlos\AppData\Local\Temp
Analysis Type	3-D
Decompose Disjoint Geometry	Yes
Enclosure and Symmetry Processing	Yes

TABLE 3
Model (C4) > Geometry > Parts

Model (C4) > Geometry > Parts		
Object Name	Solid	Solid
State	Meshed	
Graphics Properties		
Visible	Yes	
Transparency	1	
Definition		
Suppressed	No	
Stiffness Behavior	Flexible	
Coordinate System	Default Coordinate System	
Reference Temperature	By Environment	
Material		
Assignment	Si-Au mass change	Si - Au Cantilever
Nonlinear Effects	Yes	
Thermal Strain Effects	Yes	
Bounding Box		
Length X	2.e-004 m	
Length Y	1.e-004 m	1.4e-003 m
Length Z	1.25e-005 m	
Properties		

Volume	2.5e-013 m ³	3.5e-012 m ³
Mass	5.8511e-012 kg	8.1888e-011 kg
Centroid X	1.e-004 m	
Centroid Y	1.45e-003 m	7.e-004 m
Centroid Z	6.25e-006 m	
Moment of Inertia Ip1	4.9521e-021 kg·m ²	1.3376e-017 kg·m ²
Moment of Inertia Ip2	1.958e-020 kg·m ²	2.7403e-019 kg·m ²
Moment of Inertia Ip3	2.4379e-020 kg·m ²	1.3648e-017 kg·m ²
Statistics		
Nodes	428	4853
Elements	50	640
Mesh Metric	None	

Coordinate Systems

TABLE 4
Model (C4) > Coordinate Systems > Coordinate System

Object Name	<i>Global Coordinate System</i>
State	Fully Defined
Definition	
Type	Cartesian
Coordinate System ID	0.
Origin	
Origin X	0. m
Origin Y	0. m
Origin Z	0. m
Directional Vectors	
X Axis Data	[1. 0. 0.]
Y Axis Data	[0. 1. 0.]
Z Axis Data	[0. 0. 1.]

Connections

TABLE 5
Model (C4) > Connections

Object Name	<i>Connections</i>
State	Fully Defined
Auto Detection	
Generate Automatic Connection On Refresh	Yes
Transparency	
Enabled	Yes

TABLE 6
Model (C4) > Connections > Contacts

Object Name	<i>Contacts</i>
State	Fully Defined
Definition	
Connection Type	Contact
Scope	
Scoping Method	Geometry Selection
Geometry	All Bodies
Auto Detection	

Tolerance Type	Slider
Tolerance Slider	0.
Tolerance Value	3.7833e-006 m
Use Range	No
Face/Face	Yes
Face/Edge	No
Edge/Edge	No
Priority	Include All
Group By	Bodies
Search Across	Bodies
Statistics	
Connections	1
Active Connections	1

TABLE 7
Model (C4) > Connections > Contacts > Contact Regions

Object Name	<i>Contact Region</i>
State	Fully Defined
Scope	
Scoping Method	Geometry Selection
Contact	1 Face
Target	1 Face
Contact Bodies	Solid
Target Bodies	Solid
Definition	
Type	Bonded
Scope Mode	Automatic
Behavior	Program Controlled
Trim Contact	Program Controlled
Trim Tolerance	3.7833e-006 m
Suppressed	No
Advanced	
Formulation	Program Controlled
Detection Method	Program Controlled
Penetration Tolerance	Program Controlled
Elastic Slip Tolerance	Program Controlled
Normal Stiffness	Program Controlled
Update Stiffness	Program Controlled
Pinball Region	Program Controlled
Geometric Modification	
Contact Geometry Correction	None
Target Geometry Correction	None

Mesh

TABLE 8
Model (C4) > Mesh

Object Name	<i>Mesh</i>
State	Solved
Display	
Display Style	Body Color
Defaults	

Physics Preference	Mechanical
Relevance	0
Sizing	
Use Advanced Size Function	Off
Relevance Center	Fine
Element Size	Default
Initial Size Seed	Active Assembly
Smoothing	Medium
Transition	Fast
Span Angle Center	Fine
Minimum Edge Length	1.25e-005 m
Inflation	
Use Automatic Inflation	None
Inflation Option	Smooth Transition
Transition Ratio	0.272
Maximum Layers	5
Growth Rate	1.2
Inflation Algorithm	Pre
View Advanced Options	No
Patch Conforming Options	
Triangle Surface Mesher	Program Controlled
Patch Independent Options	
Topology Checking	No
Advanced	
Number of CPUs for Parallel Part Meshing	Program Controlled
Shape Checking	Standard Mechanical
Element Midside Nodes	Program Controlled
Straight Sided Elements	No
Number of Retries	Default (4)
Extra Retries For Assembly	Yes
Rigid Body Behavior	Dimensionally Reduced
Mesh Morphing	Disabled
Defeaturing	
Pinch Tolerance	Please Define
Generate Pinch on Refresh	No
Automatic Mesh Based Defeaturing	On
Defeaturing Tolerance	Default
Statistics	
Nodes	5281
Elements	690
Mesh Metric	None

Modal (C5)

TABLE 9
Model (C4) > Analysis

Object Name	<i>Modal (C5)</i>
State	Solved
Definition	
Physics Type	Structural
Analysis Type	Modal
Solver Target	Mechanical APDL

Options	
Environment Temperature	22. °C
Generate Input Only	No

TABLE 10
Model (C4) > Modal (C5) > Initial Condition

Object Name	<i>Pre-Stress (None)</i>
State	Fully Defined
Definition	
Pre-Stress Environment	None

TABLE 11
Model (C4) > Modal (C5) > Analysis Settings

Object Name	<i>Analysis Settings</i>
State	Fully Defined
Options	
Max Modes to Find	6
Limit Search to Range	No
Solver Controls	
Damped	Yes
Solver Type	Program Controlled
Rotordynamics Controls	
Coriolis Effect	Off
Campbell Diagram	Off
Output Controls	
Stress	No
Strain	No
Nodal Forces	No
Calculate Reactions	No
General Miscellaneous	No
Damping Controls	
Stiffness Coefficient Define By	Direct Input
Stiffness Coefficient	0.
Mass Coefficient	0.
Analysis Data Management	
Solver Files Directory	F:\Dropbox\BSc Mechatronics - SDU\Classes\6 MC\Thesis\ANSYS\cantilever_3_files\dp0\SYS-6\MECH\
Future Analysis	None
Scratch Solver Files Directory	
Save MAPDL db	No
Delete Unneeded Files	Yes
Solver Units	Active System
Solver Unit System	mks

TABLE 12
Model (C4) > Modal (C5) > Loads

Object Name	<i>Fixed Support</i>
State	Fully Defined
Scope	

Scoping Method	Geometry Selection
Geometry	1 Face
Definition	
Type	Fixed Support
Suppressed	No

Solution (C6)

TABLE 13
Model (C4) > Modal (C5) > Solution

Object Name	<i>Solution (C6)</i>
State	Solved
Adaptive Mesh Refinement	
Max Refinement Loops	1.
Refinement Depth	2.
Information	
Status	Done
Post Processing	
Calculate Beam Section Results	No

The following bar chart indicates the frequency at each calculated mode.

FIGURE 1
Model (C4) > Modal (C5) > Solution (C6)

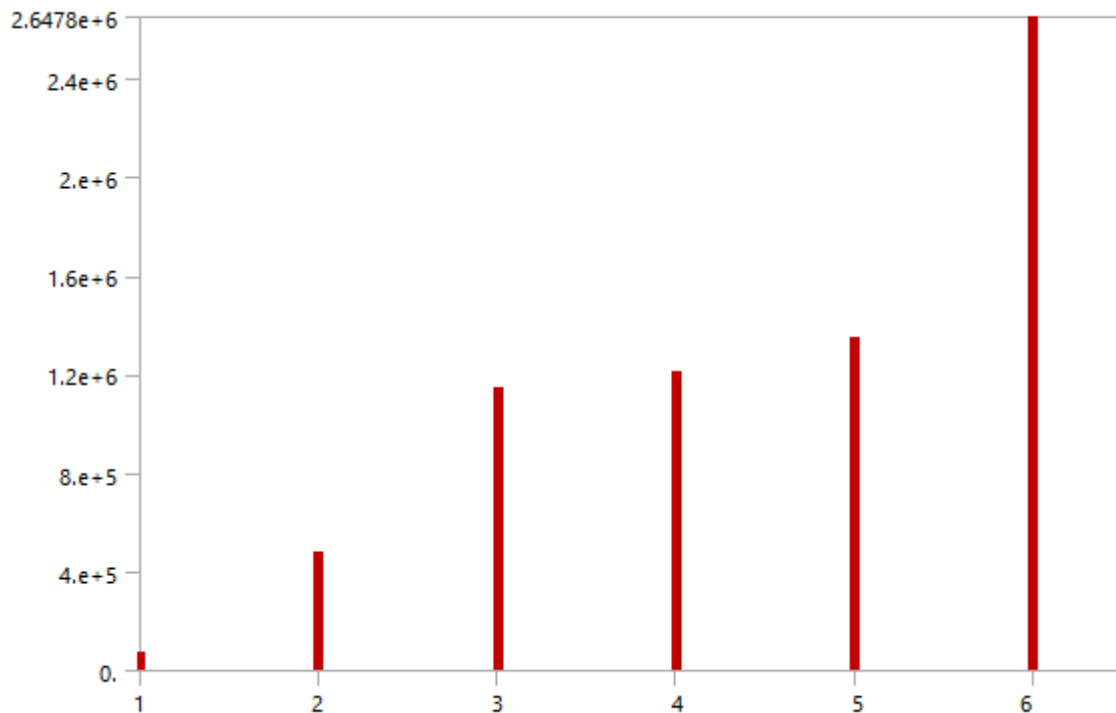


TABLE 14
Model (C4) > Modal (C5) > Solution (C6)

Mode	Damped Frequency [Hz]	Stability [Hz]	Modal Damping Ratio	Logarithmic Decrement
1.	76968	0.	0.	0.
2.	4.821e+005			

3.	1.142e+006			
4.	1.2093e+006			
5.	1.3503e+006			
6.	2.6478e+006			

TABLE 15
Model (C4) > Modal (C5) > Solution (C6) > Solution Information

Object Name	<i>Solution Information</i>
State	Solved
Solution Information	
Solution Output	Solver Output
Newton-Raphson Residuals	0
Update Interval	2.5 s
Display Points	All
FE Connection Visibility	
Activate Visibility	Yes
Display	All FE Connectors
Draw Connections Attached To	All Nodes
Line Color	Connection Type
Visible on Results	No
Line Thickness	Single
Display Type	Lines

TABLE 16
Model (C4) > Modal (C5) > Solution (C6) > Results

Object Name	Total Deformation		Total Deformation 2	
State	Solved			
Scope				
Scoping Method	Geometry Selection			
Geometry	All Bodies			
Definition				
Type	Total Deformation			
Mode	1.		2.	
Sweeping Phase	0. °			
Identifier				
Suppressed	No			
Results				
Minimum	0. m			
Maximum	2.1381e+005 m			
Minimum Occurs On	Solid			
Maximum Occurs On	Solid			
Information				
Damped Frequency	76968 Hz		4.821e+005 Hz	
Stability	0. Hz			
Modal Damping Ratio	0.			
Logarithmic Decrement	0.			

TABLE 17
Model (C4) > Modal (C5) > Solution (C6) > Total Deformation

Mode	Damped Frequency [Hz]	Stability [Hz]	Modal Damping Ratio	Logarithmic Decrement
1.	76968	0.	0.	0.
2.	4.821e+005			
3.	1.142e+006			

4.	1.2093e+006			
5.	1.3503e+006			
6.	2.6478e+006			

TABLE 18
Model (C4) > Modal (C5) > Solution (C6) > Total Deformation 2

Mode	Damped Frequency [Hz]	Stability [Hz]	Modal Damping Ratio	Logarithmic Decrement
1.	76968	0.	0.	0.
2.	4.821e+005			
3.	1.142e+006			
4.	1.2093e+006			
5.	1.3503e+006			
6.	2.6478e+006			

Material Data

Si-Au mass change

TABLE 19
Si-Au mass change > Constants

Density	23.404 kg m ⁻³
---------	---------------------------

TABLE 20
Si-Au mass change > Isotropic Elasticity

Temperature C	Young's Modulus Pa	Poisson's Ratio	Bulk Modulus Pa	Shear Modulus Pa
	1.7e+011	0.24	1.0897e+011	6.8548e+010

Si - Au Cantilever

TABLE 21
Si - Au Cantilever > Constants

Density	23.397 kg m ⁻³
---------	---------------------------

TABLE 22
Si - Au Cantilever > Isotropic Elasticity

Temperature C	Young's Modulus Pa	Poisson's Ratio	Bulk Modulus Pa	Shear Modulus Pa
	1.7e+011	0.24	1.0897e+011	6.8548e+010

7.4 MatLab Code

PARAMETERS INSERTION.....	77
CALCULATIONS	77
SPRING CONSTANT K CALCULATIONS	77
CANTILEVER MASS CALCULATIONS BASED ON THE HARMONIC OSCILLATOR EQUATION.....	78
CALCULATION OF FINAL FREQUENCY DEPPENDING ON CANTILEVER TYPE	78
SURFACE AREA VALUE	78
FORCE PER AREA CALCULATION (SIGMA)	79
DENSITY OF CANTILEVER CALCULATION	79
CALCULATIONS FOR DISPLACEMENT OF CANTILEVER AT INITIAL RESONANCE FREQUENCY.....	79
CALCULATIONS FOR DISPLACEMENT OF CANTILEVER AT FINAL RESONANCE FREQUENCY	80
CALCULATIONS FOR LASER DISPLACEMENT AT THE DETECTOR AT A CHOSEN DISTANCE ACCORDING TO PAPER	80
CALCULATIONS FOR PIEZOSENSING CIRCUIT (CURRENT BRIDGE).....	80
GENERAL CALCULATIONS FOR OPTICS	81
GAUSSIAN PROPAGATION THROUGH LENSES - GRAPHIC VISUALIZATION	82
CALCULATIONS OF EXPERIMENTAL MASS CHANGE	83

```
% MEMS biosensor Calculator
```

7.4.1 Parameters Insertion

```
clear all; clc;

%INPUTS INSERTION AND GLOBAL VARIABLES DECLARATION

length = 1500*10^(-6);
width = 200*10^(-6);
height = 12.5*10^(-6);
poisson = 0.22;
young_modulus = 170*10^9;
resonant_frequency = 7.8*10^3;
laser_wavelength = 632.8*10^(-9);
laser_poweroutput = 1*10^(-3);
laser_divergence = 0.00123;
laser_spotr = 1*10^(-3);
force = 600*10^(-18)*9.81; % Using smallest measured amount
distance_pdetector = 0.406971;
I_moment = (width*height^3)/12;
B = (length)^3;
area = length*width;
X_area = width*height;
piezo_capacitance = 112*10^(-12);
piezo_impedance = 175*10^3;
gain = 10;
syms x y z a b c d e f g h u
```

7.4.2 CALCULATIONS

7.4.3 Spring constant k calculations

```
fprintf('The cantilever spring constant K, is (N/m) = ');
solve (u==3*young_modulus*I_moment/B);
```

```
K = double(ans);
K
```

The cantilever spring constant K, is (N/m) =
K =

4.5370e-05

7.4.4 Cantilever mass calculations based on the harmonic oscillator equation

```
fprintf('The mass of the cantilever is (kg) = ');
solve(resonant_frequency == 1/2*pi*sqrt(K/y));
mass = double(ans);
mass
```

```
final_mass = mass + 6.74*10^(-16); %Assumed (kg)
initial_frequency = resonant_frequency;
mass_captured_cadeverine = final_mass - mass;
```

The mass of the cantilever is (kg) =
mass =

1.8400e-12

7.4.5 Calculation of final frequency depending on cantilever type

```
fprintf('The final frequency of the cantilever is (Hz) = ');
solve (mass_captured_cadeverine == (K)/(0.96*pi^2)*(1/(z^2)-1/(initial_frequency^2)), z,
'PrincipalValue', true);
final_frequency = double(ans);
final_frequency = abs(final_frequency);
final_frequency
fprintf('The shift in frequency due to mass change of the cantilever is (Hz) = ');
shift_frequency = resonant_frequency-final_frequency;
shift_frequency
```

The final frequency of the cantilever is (Hz) =
final_frequency =

7.7668e+03

The shift in frequency due to mass change of the cantilever is (Hz) =
shift_frequency =

33.1850

7.4.6 Surface area value

```
fprintf('The surface area of the cantilever is (m) = ');
area
```

The surface area of the cantilever is (m) =
area =

3.0000e-07

7.4.7 Force per area calculation (sigma)

```
fprintf('The force per unit area is (N/m^2 - Pa) = ');  
solve (force == (a*x_area*(1-poisson))/length);  
sigma = double(ans);  
sigma  
fprintf('The deflection of the cantilever due to mass change is of (m) = ');  
deflection_masschange = (4*length^2*sigma*(1-poisson))/(young_modulus*height^2);  
deflection_masschange
```

The force per unit area is (N/m² - Pa) =
sigma =

2.1590e-07

The deflection of the cantilever due to mass change is of (m) =
deflection_masschange =

1.2973e-10

7.4.8 Density of cantilever calculation

```
fprintf('The density of the cantilever material is in average (kg/m^3) = ');  
volume = area*height;  
mass/volume;  
density = double(ans);  
density  
final_mass/volume;  
density_tip_mass_change = double(ans);  
density_tip_mass_change
```

The density of the cantilever material is in average (kg/m³) =
density =

23.3967

density_tip_mass_change =

23.4053

7.4.9 Calculations for displacement of cantilever at initial resonance frequency

```
fprintf('The measured distance of displacement at initial frequency is (m) = ');  
solve(resonant_frequency==1/(2*pi)*sqrt(9.81/f));  
deflection_resonance_frequency=double(ans);  
deflection_resonance_frequency
```

The measured distance of displacement at initial frequency is (m) =
deflection_resonance_frequency =

4.0843e-09

7.4.10 Calculations for displacement of cantilever at final resonance frequency

```
fprintf('The measured distance of displacement at resulting frequency is (m) = ');  
solve(final_frequency==1/(2*pi)*sqrt(9.81/g));  
deflection_final_frequency=double(ans);  
deflection_final_frequency
```

The measured distance of displacement at resulting frequency is (m) =
deflection_final_frequency =

4.1193e-09

7.4.11 Calculations for laser displacement at the detector at a chosen distance according to paper

```
fprintf('The measured distance of displacement of the reflected laser at the detector is  
(m) = ');  
solve(deflection_masschange*3*distance_pdetector/length == e);  
displacement2_at_detector = double(ans);  
displacement2_at_detector
```

The measured distance of displacement of the reflected laser at the detector is (m) =
displacement2_at_detector =

1.0560e-07

7.4.12 Calculations for piezosensing circuit (current bridge)

```
fprintf('The values for the circuit are = ');  
R1_value=piezo_impedance;  
total_resistance=(1/(1/R1_value+1/piezo_impedance));  
total_resistance  
R2_value=gain*total_resistance;  
R2_value  
solve(-  
1/(2*pi*(resonant_frequency*10^3)*piezo_capacitance)==2*pi*(resonant_frequency*10^3)*d); %Here  
e Xc=Xl  
parasitic_inductance=abs(double(ans));  
parasitic_inductance  
f_circuit=abs(1/(2*pi*sqrt(piezo_capacitance*parasitic_inductance)));  
f_circuit  
Vin_opamp=1.7; % For example  
Vout_opamp=(R2_value/total_resistance*Vin_opamp);  
Vout_opamp
```

The values for the circuit are =
total_resistance =

87500

R2_value =

875000

parasitic_inductance =

3.7173e-06

f_circuit =

7800000

vout_opamp =

17

7.4.13 General calculations for Optics

```
syms r j
theta=laser_divergence;
w_0=(laser_wavelength)/(pi*theta);
fprintf('The beam waist radius w_0 is (m) = ');
w_0
d_0=2*w_0;
fprintf('Minimal beam diameter is (m) = ');
d_0
z_0=pi*w_0^2/laser_wavelength;
fprintf('The Rayleigh length is (m) = ');
z_0
I_0=laser_poweroutput/(pi*w_0^2/2); %calculates peak intensity on beam axis
l=I_0*exp(-(2*r^2)/w_0^2); %intensity curve of laser beam over distance
m=w_0*sqrt(1+(j/z_0)^2); %change of beam waist with distance

figure(2);
fplot(l,[-0.0005 0.0005],'g'); %plots intensity curve of laser beam over distance
figure(3);
fplot(m,[-0.01 0.01],'m'); %plots change of beam waist with distance
```

The beam waist radius w_0 is (m) =

w_0 =

1.6376e-04

Minimal beam diameter is (m) =

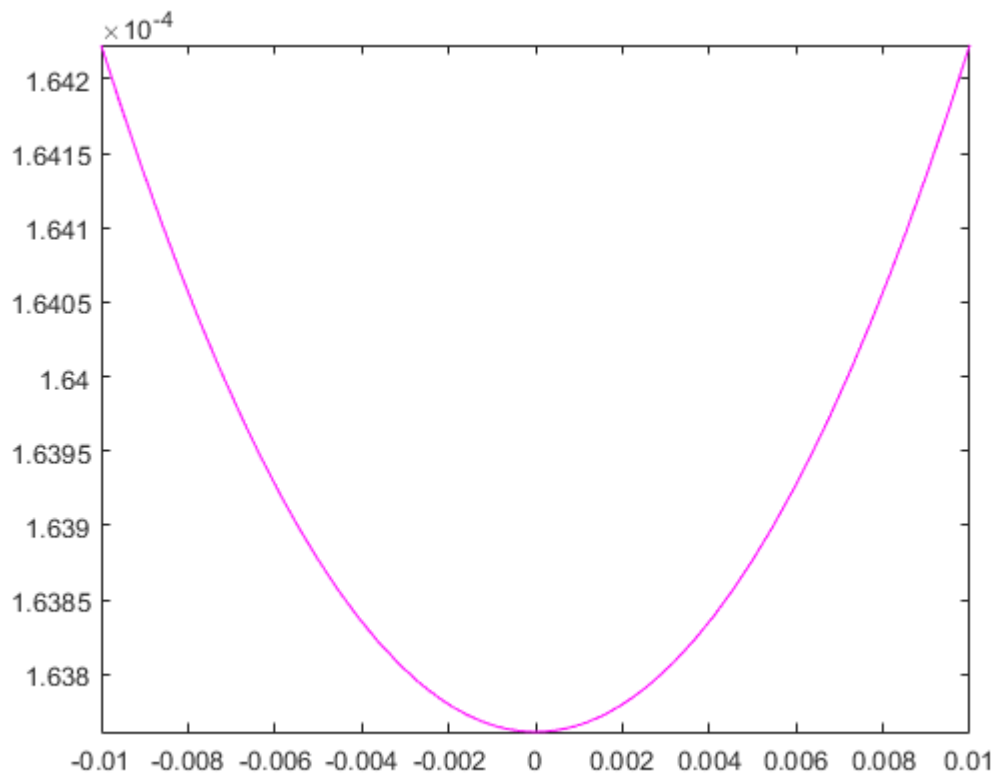
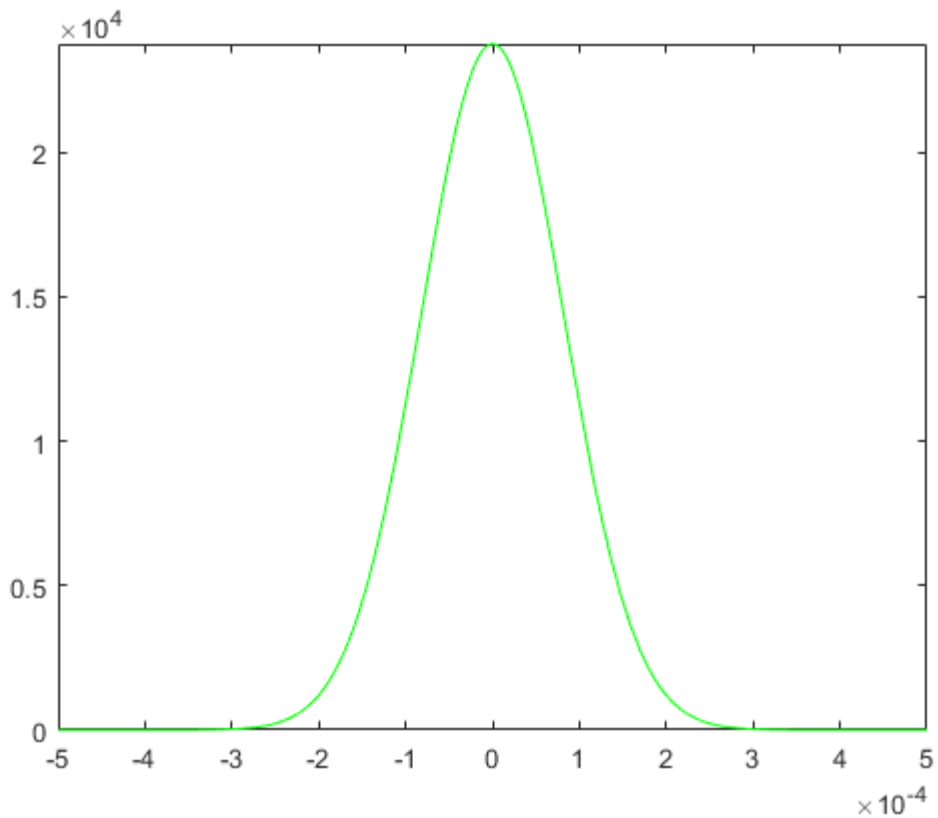
d_0 =

3.2752e-04

The Rayleigh length is (m) =

z_0 =

0.1331

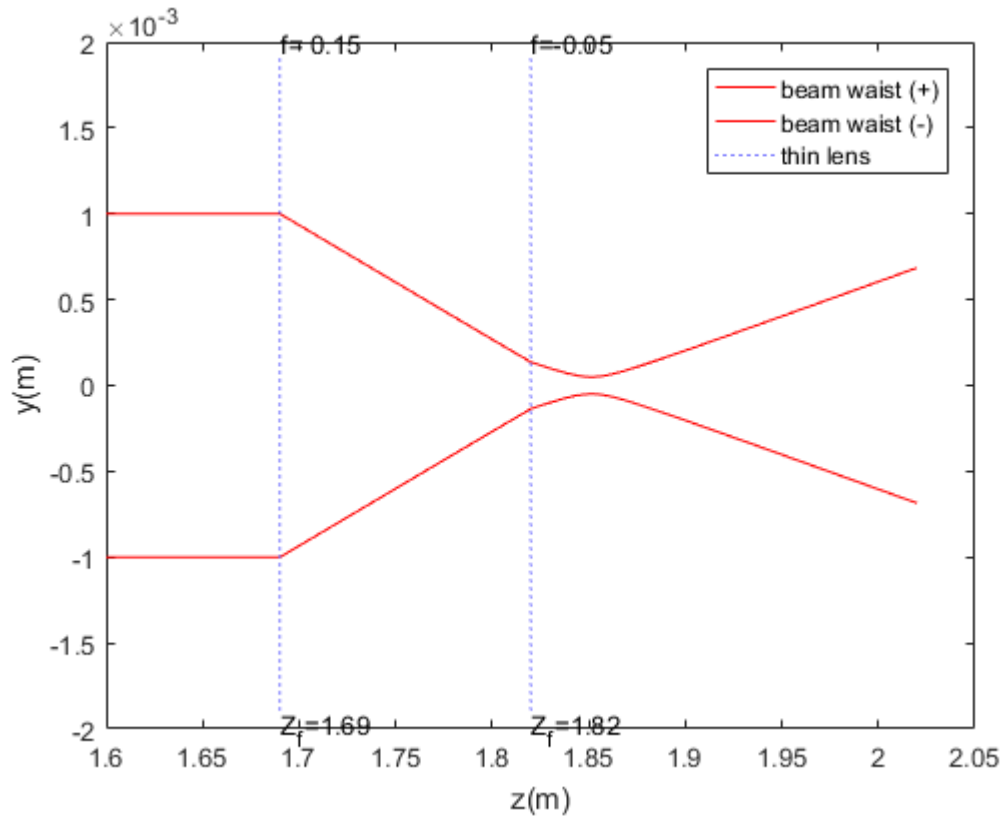


7.4.14 Gaussian propagation through lenses - graphic visualization

%based on script from
<http://www.mathworks.com/matlabcentral/fileexchange/37436-gaussian-beam-propagation-through-a-series-of-thin-lenses>

```
%Gaussian_Propagation(wavelength,beam_position,plot_start_position,[position_lens1
position_lens2],[focal_length_lens1 focal_length_lens2])
Gaussian_Propagation(laser_wavelength,laser_spotr,1.6,[1.690 1.820],[0.150 -0.050])
```

waist position from last lens:0.031333
waist size:4.9699e-05



7.4.15 Calculations of experimental mass change

```
%Optical setup
frequency0 = 7700;
frequency1 = 7200;
mass_cadaverine_optics = (K)/(0.96*pi^2)*(1/(frequency1^2)-1/(frequency0^2));
fprintf('The mass of cadaverine detected by the optical setup is of (Kg) = ');
mass_cadaverine_optics

%Electrical setup
values_voltage=[1-0.246,1-0.255,1-0.2528,1-0.269,1-0.267,1-0.273,1-0.29,1-0.291,1-0.289];
Times=[10,20,30,40,50,60,90,120,180];
first_value = 1-0.240;
for i=1:9
    mass_cadaverine_piezo = (K)/(0.96*pi^2)*(1/(values_voltage(i)^2)-1/(first_value^2));
    fprintf('At time (s) =');
    Times(i)
    fprintf('The mass of cadaverine detected by the piezo sensing setup is of (Kg) =');
    mass_cadaverine_piezo
end

%Sensitivity calculations

%AFM
```



```

Delta_f = 850;
Delta_m = 6.74*10^(-16);
Sensitivity = Delta_f/Delta_m;
fprintf('The sensitivity of the AFM is (Hz/Kg) =');
Sensitivity
%Optical
Delta_f = frequency0-frequency1;
Delta_m = mass_cadaverine_optics;
Sensitivity = Delta_f/Delta_m;
fprintf('The sensitivity of the Optical setup is (Hz/Kg) =');
Sensitivity
%Piezo sensing
Delta_f = 192;
Delta_m = mass_cadaverine_piezo;
Sensitivity = Delta_f/Delta_m;
fprintf('The sensitivity of the Piezo sensing setup is (Hz/Kg) =');
Sensitivity

%Accuracy calculations
%Optical in percentage
Accuracy_optics=abs(mass_cadaverine_optics-(6.74*10^(-16)))/(6.74*10^(-16));
fprintf('The accuracy of the Optical setup is =');
Accuracy_optics
%Piezo sensing in percentage
Accuracy_piezo=abs(mass_cadaverine_piezo-(6.74*10^(-16)))/(6.74*10^(-16));
fprintf('The accuracy of the Piezo sensing setup is =');
Accuracy_piezo

```

The mass of cadaverine detected by the optical setup is of (Kg) =
mass_cadaverine_optics =

1.1607e-14

At time (s) =
ans =

10

The mass of cadaverine detected by the piezo sensing setup is of (Kg) =
mass_cadaverine_piezo =

1.3247e-07

At time (s) =
ans =

20

The mass of cadaverine detected by the piezo sensing setup is of (Kg) =
mass_cadaverine_piezo =

3.3720e-07

At time (s) =
ans =

30

The mass of cadaverine detected by the piezo sensing setup is of (Kg) =
mass_cadaverine_piezo =

2.8647e-07

At time (s) =
ans =

40

The mass of cadaverine detected by the piezo sensing setup is of (Kg) =
mass_cadaverine_piezo =

6.7082e-07

At time (s) =
ans =

50

The mass of cadaverine detected by the piezo sensing setup is of (Kg) =
mass_cadaverine_piezo =

6.2199e-07

At time (s) =
ans =

60

The mass of cadaverine detected by the piezo sensing setup is of (Kg) =
mass_cadaverine_piezo =

7.6970e-07

At time (s) =
ans =

90

The mass of cadaverine detected by the piezo sensing setup is of (Kg) =
mass_cadaverine_piezo =

1.2088e-06

At time (s) =
ans =

120

The mass of cadaverine detected by the piezo sensing setup is of (Kg) =
mass_cadaverine_piezo =

1.2356e-06

At time (s) =
ans =

180

The mass of cadaverine detected by the piezo sensing setup is of (Kg) =
mass_cadaverine_piezo =

1.1821e-06

The sensitivity of the AFM is (Hz/Kg) =
Sensitivity =

1.2611e+18

The sensitivity of the Optical setup is (Hz/Kg) =
Sensitivity =

4.3079e+16

The sensitivity of the Piezo sensing setup is (Hz/Kg) =
Sensitivity =

1.6243e+08

The accuracy of the Optical setup is =
Accuracy_optics =

16.2204

The accuracy of the Piezo sensing setup is =
Accuracy_piezo =

1.7538e+09

Published with MATLAB® R2016a

7.5 Risk assessment

Risk-Management-Plan (RIM-Plan)

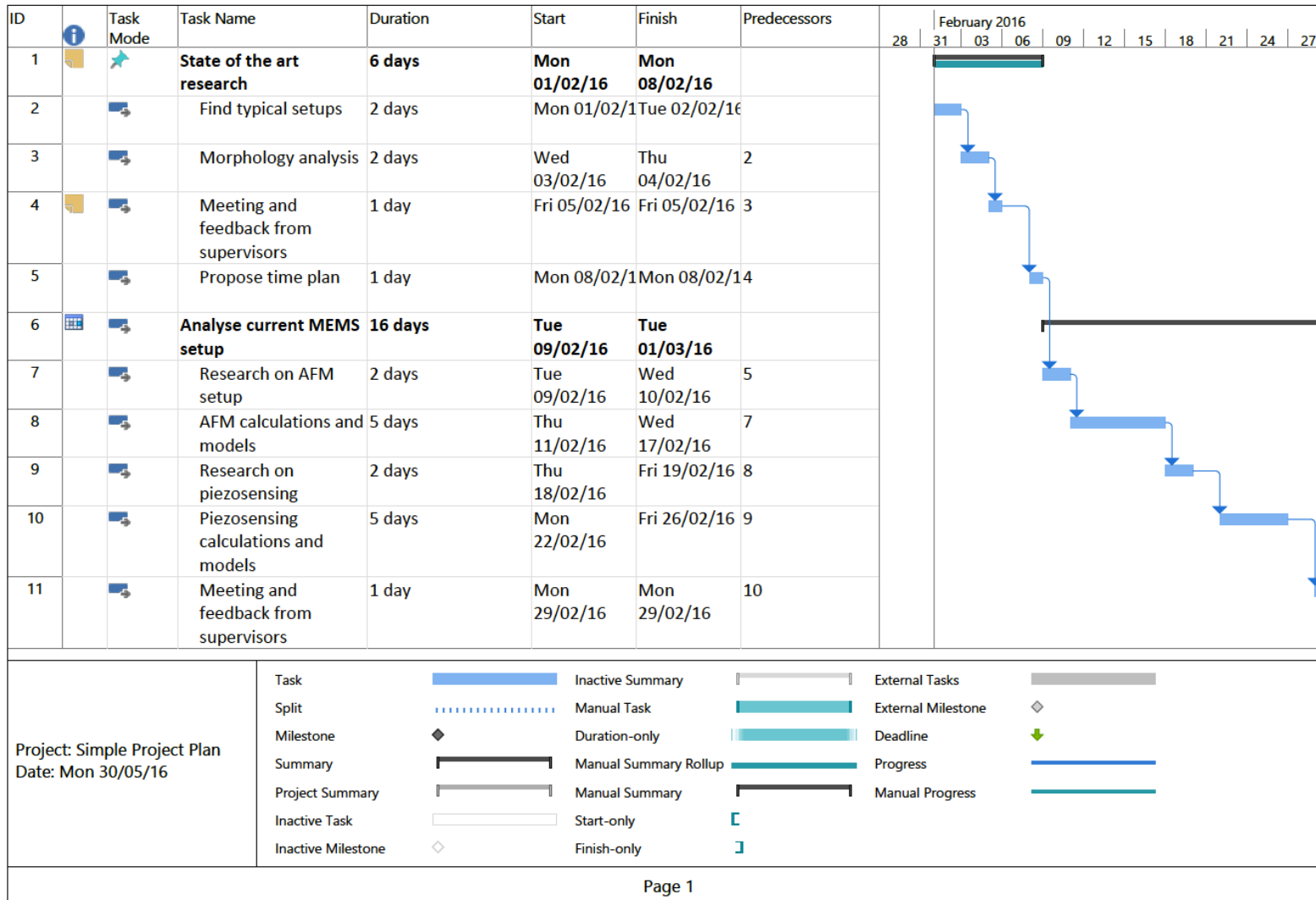
Project	Author	Date	Document	Vers.
MEMS biosensor for detection of	Carlos Costa	02.01.2016		1














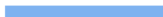











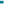






Identification					ANALYSIS					
Seq. No.	Category	Description of risk	Trigger point of risk	Effect on the project	before action				1. description of the solution	2. responsible person
					Impact	Probability in %	Risk Level	Due date for solution		
1	Mechanical	Direct physical damage to parts	Assembly of prototype	Assembly delay, additional costs	5	60%	3.0		Use of extra parts	Carlos
2	Mechanical	Piezocantilever sensitivity not adequate	Assembly of prototype	Requirements not met	5	20%	1.0		Choose alternative type of setup and compare results	Carlos
3	Mechanical	Production/Acquisition of parts too expensive	Designing	Not able to use anticipated parts	4	60%	2.0		Order on time, use test parts instead of final ones	Carlos
4	Mechanical	Cantilever and piezo not easily assembled	Assembly of prototype	Requirements not met	4	60%	2.0		Redesign/fit the parts with an input from supervisors	Carlos
5	Mechanical	Laser displacement not adequate for photodiode detector	Test of electronics and optics	More time needed, additional cost	2	40%	1.0		Adapt current setup/parts with input from supervisors	Carlos
6	Electrical	Acquisition of parts too expensive	Designing	Not able to use anticipated parts	5	40%	2.0		Use of test parts instead of final ones	Carlos
7	Electrical	Parts damaged	Test of electronics and optics	More time needed, additional cost	5	60%	3.0		Use of extra parts, request assistance from possible sponsors	Carlos
8	Electrical	Circuit not working as intended	Test of electronics and optics	More time needed	2	60%	2.0		Request assistance from supervisors or external experts	Carlos
9	Electrical	Laser related injury	Assembly of prototype	Temporary or permanent injury	5	20%	1.0		Prevention: Attend laser safety course; Use protective measures;	Carlos
10	Electrical	Electric components not compatible	Test of electronics and optics	More time needed, additional cost	5	40%	2.0		Get an overview of parts get info early or procure further funding to order compatible parts	Carlos
11	Electrical	Noise from unwanted sources	Test of electronics and optics	More time needed	4	60%	2.0		Request assistance from supervisors or experts to identify sources and if possible redesign setup to minimize them	Carlos
12	Electrical	Risk of electrocution	Assembly of prototype	Temporary or permanent injury	5	20%	1.0		Prevention: LAUS course and use of protective measures	Carlos
13	Production	Electric components late failure	Integration tests	More time needed, additional cost	4	40%	2.0		Order compatible equivalents	Carlos
14	Production	Final product not behaving according to simulations/expectations	Integration tests	Risk of requirements not met/Further research needed	5	40%	2.0		Analyze problem and if needed redesign setup with assistance from supervisors/experts	Carlos
15	Production	Final product not able to give any output for comparison requirements	Integration tests	Requirements not met	5	40%	2.0		Analyze problem and if needed redesign setup with assistance from supervisors/experts	Carlos
16	Marketing	Final product not meeting market / Proposed requirements for portability	Final review	Requirements not met	5	40%	2.0		Early input from supervisors on requirements	Carlos










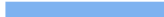


















Unmitigated Risks	Risk level 3	2
	Risk level 2	10
	Risk level 1	4






























Probability	Impact				
	1	2	3	4	5
0%	0	0	0	0	0
20%	1	1	1	1	1
40%	1	1	1	2	2
60%	1	2	2	2	3
80%	1	2	2	3	3
100%	1	2	3	3	3

7.6 Gantt Chart



ID		Task Mode	Task Name	Duration	Start	Finish	Predecessors	February 2016											
								28	31	03	06	09	12	15	18	21	24	27	
12			Perform risk assessment and update time plan	1 day	Tue 01/03/16	Tue 01/03/16	11												
13			Simulations of proposed setups	6 days	Tue 01/03/16	Tue 08/03/16													
14			AFM Optical setup - cantilever frequencies in ANSYS	3 days	Tue 01/03/16	Thu 03/03/16	11												
15			Piezosensing setup - Multisim model	3 days	Fri 04/03/16	Tue 08/03/16	14												
16			Acceptance tests for model verification	24 days	Wed 09/03/16	Mon 11/04/16													
17			Design piezo driven setup	3 days	Wed 09/03/16	Fri 11/03/16	15												
18			Perform resonant frequencies measurements	7 days	Mon 14/03/16	Tue 22/03/16	17												
19			Design optical setup	3 days	Wed 23/03/16	Fri 25/03/16	18												
20			Perform resonant frequencies	7 days	Mon 28/03/16	Tue 05/04/16	19												
21			Meeting and result discussion with supervisors	1 day	Wed 06/04/16	Wed 06/04/16	20												
<div><div>Project: Simple Project Plan Date: Mon 30/05/16</div><div><div><div>Task</div><div></div></div><div><div>Split</div><div></div></div><div><div>Milestone</div><div></div></div><div><div>Summary</div><div></div></div><div><div>Project Summary</div><div></div></div><div><div>Inactive Task</div><div></div></div><div><div>Inactive Milestone</div><div></div></div><div><div>Inactive Summary</div><div></div></div><div><div>Manual Task</div><div></div></div><div><div>Duration-only</div><div></div></div><div><div>Manual Summary Rollup</div><div></div></div><div><div>Manual Summary</div><div></div></div><div><div>Start-only</div><div></div></div><div><div>Finish-only</div><div></div></div><div><div>External Tasks</div><div></div></div><div><div>External Milestone</div><div></div></div><div><div>Deadline</div><div></div></div><div><div>Progress</div><div></div></div><div><div>Manual Progress</div><div></div></div></div></div>																			
Page 2																			

ID		Task Mode	Task Name	Duration	Start	Finish	Predecessors	February 2016													
22			Update risk assessment and time plan	1 day	Thu 07/04/16	Thu 07/04/16	21	28	31	03	06	09	12	15	18	21	24	27			
23			Prototype setup for functionalized cantilevers	31 days	Fri 08/04/16	Fri 20/05/16															
24			Design/Adapt setups based on previous results	3 days	Fri 08/04/16	Tue 12/04/16	22														
25			Update risk assessment and time plan	1 day	Wed 13/04/16	Wed 13/04/16	24														
26			Build final optical setup, perform integration tests	10 days	Thu 14/04/16	Wed 27/04/16	25														
27			Treat obtained data	3 days	Thu 28/04/16	Mon 02/05/16	26														
28			Build final piezosensing setup, perform integration tests	10 days	Tue 03/05/16	Mon 16/05/16	27														
29			Treat obtained data	3 days	Tue 17/05/16	Thu 19/05/16	28														
Project: Simple Project Plan Date: Mon 30/05/16			Task		Inactive Summary		External Tasks														
			Split		Manual Task		External Milestone														
			Milestone		Duration-only		Deadline														
			Summary		Manual Summary Rollup		Progress														
			Project Summary		Manual Summary		Manual Progress														
			Inactive Task		Start-only																
			Inactive Milestone		Finish-only																
			Page 3																		

ID		Task Mode	Task Name	Duration	Start	Finish	Predecessors	28	February 2016										31	03	06	09	12	15	18	21	24	27								
30			Meeting and result discussion with supervisors	1 day	Fri 20/05/16	Fri 20/05/16	29																													
31			Final documentation and report production	16 days	Wed 11/05/16	Wed 01/06/16																														
32			Produce main body of report	11 days	Wed 11/05/16	Wed 25/05/16																														
33			Create appendices	1 day	Thu 26/05/16	Thu 26/05/16	32																													
34			Formating	1 day	Fri 27/05/16	Fri 27/05/16	33																													
35			Meeting with supervisors and final remarks	1 day	Mon 30/05/16	Mon 30/05/16	34																													
36			Last revision and Printing	1 day	Tue 31/05/16	Tue 31/05/16	35																													
37			Delivery	1 day	Wed 01/06/16	Wed 01/06/16	36																													
Project: Simple Project Plan Date: Mon 30/05/16			Task		Inactive Summary		External Tasks																													
			Split		Manual Task		External Milestone																													
			Milestone		Duration-only		Deadline																													
			Summary		Manual Summary Rollup		Progress																													
			Project Summary		Manual Summary		Manual Progress																													
			Inactive Task		Start-only																															
			Inactive Milestone		Finish-only																															
Page 4																																				

